

# Anatomy of $B \rightarrow K\eta^{(\prime)}$ decays in different mixing schemes and effects of next-to-leading order contributions in the perturbative QCD approach

Ying-Ying Fan, Wen-Fei Wang, Shan Cheng, and Zhen-Jun Xiao <sup>a</sup>,

*Department of Physics and Institute of Theoretical Physics,  
Nanjing Normal University, Nanjing, Jiangsu 210023, P.R.China*

(Dated: September 12, 2018)

## Abstract

In this paper we perform a comprehensive study of the four  $B \rightarrow K\eta^{(\prime)}$  decays in the perturbative QCD (pQCD) factorization approach. We calculate the CP-averaged branching ratios and CP-violating asymmetries of  $B \rightarrow K\eta^{(\prime)}$  decays in the ordinary  $\eta$ - $\eta'$ , the  $\eta$ - $\eta'$ - $G$ , and the  $\eta$ - $\eta'$ - $G$ - $\eta_c$  mixing schemes. Besides the full leading order (LO) contributions, all currently known next-to-leading order (NLO) contributions to  $B \rightarrow K\eta^{(\prime)}$  decays in the pQCD approach are taken into account. From our calculations and phenomenological analysis, we find the following. (a) The NLO contributions in general can provide significant enhancements to the LO pQCD predictions for the decay rates of the two  $B \rightarrow K\eta'$  decays, around 70%–89% in magnitude, but result in relatively small changes to  $Br(B \rightarrow K\eta)$ . (b) Although the NLO pQCD predictions in all three considered mixing schemes agree well with the data within one standard deviation, those pQCD predictions in the  $\eta$ - $\eta'$ - $G$  mixing scheme provide the best interpretation for the measured pattern of  $Br(B \rightarrow K\eta^{(\prime)})$ :  $Br(B^0 \rightarrow K^0\eta) \approx 1.13 \times 10^{-6}$ ,  $Br(B^0 \rightarrow K^0\eta') \approx 66.5 \times 10^{-6}$ ,  $Br(B^\pm \rightarrow K^\pm\eta) \approx 2.36 \times 10^{-6}$ , and  $Br(B^\pm \rightarrow K^\pm\eta') \approx 67.3 \times 10^{-6}$ , which agree perfectly with the measured values. (c) The NLO pQCD predictions for the CP-violating asymmetries for the four considered decays are also in good consistent with the data. (d) The newly known NLO contribution to the relevant form factors  $\mathcal{M}_{FF}$  can produce about a 20% enhancement to the branching ratios  $Br(B \rightarrow K\eta')$ , which plays an important role in closing the gap between the pQCD predictions and the relevant data. (e) The general expectations about the relative strength of the LO and NLO contributions from different sources are examined and confirmed by explicit numerical calculations.

PACS numbers: 13.25.Hw, 12.38.Bx, 14.40.Nd

---

<sup>a</sup> Electronic address: xiaozhenjun@njnu.edu.cn

## I. INTRODUCTION

Since the first observation of unexpectedly large branching ratios for  $B \rightarrow K\eta'$  decays was reported by CLEO in 1997 [1], the four  $B \rightarrow K\eta^{(\prime)}$  decays have been a “hot” topic for a long time. Although many physicists have made great efforts to explain the pattern of very large branching ratios  $Br(B \rightarrow K\eta')$  and very small branching ratios  $Br(B \rightarrow K\eta)$  [2–9], it is still difficult to understand such a pattern in the framework of the standard model(SM).

On the experimental side, the branching ratios of the four  $B \rightarrow K\eta^{(\prime)}$  decays have been measured with high precision [10, 11],

$$\begin{aligned} Br(B^0 \rightarrow K^0\eta) &= (1.23_{-0.24}^{+0.27}) \times 10^{-6}, \\ Br(B^0 \rightarrow K^0\eta') &= (66.1 \pm 3.1) \times 10^{-6}, \\ Br(B^\pm \rightarrow K^\pm\eta) &= (2.36_{-0.21}^{+0.22}) \times 10^{-6}, \\ Br(B^\pm \rightarrow K^\pm\eta') &= (71.1 \pm 2.6) \times 10^{-6}, \end{aligned} \quad (1)$$

For the relevant CP-violating asymmetries, the currently known experimental measurements are [10, 11]

$$\begin{aligned} \mathcal{A}_{CP}^{dir}(B^0 \rightarrow K^0\eta') &= (1 \pm 9)\%, \\ \mathcal{A}_{CP}^{mix}(B^0 \rightarrow K^0\eta') &= (64 \pm 11)\%, \\ \mathcal{A}_{CP}^{dir}(B^\pm \rightarrow K^\pm\eta) &= (-37 \pm 8)\%, \\ \mathcal{A}_{CP}^{dir}(B^\pm \rightarrow K^\pm\eta') &= (1.3_{-1.7}^{+1.6})\%, \end{aligned} \quad (2)$$

On the theory side, these decays were calculated recently in Ref. [12] by employing the perturbative QCD (pQCD) factorization approach[9] and using the ordinary Feldmann-Kroll-Stech (FKS)  $\eta - \eta'$  mixing scheme [13], with the inclusion of the partial next-to-leading order (NLO) contributions, i.e., the QCD vertex corrections, the quark-loops, and the chromomagnetic penguins  $O_{8g}$ . In Ref. [12] the authors found that the NLO contributions can provide a 70% enhancement to the leading order (LO) pQCD predictions for  $Br(B \rightarrow K\eta')$ , but also produce a 30% reduction to the LO pQCD predictions for  $Br(B \rightarrow K\eta)$  [12]; numerically,  $Br(B^0 \rightarrow K^0\eta) \approx 2.1 \times 10^{-6}$ ,  $Br(B^0 \rightarrow K^0\eta') \approx 50.3 \times 10^{-6}$ ,  $Br(B^+ \rightarrow K^+\eta) \approx 3.2 \times 10^{-6}$ , and  $Br(B^\pm \rightarrow K^\pm\eta') \approx 51.0 \times 10^{-6}$ . Although the differences between the pQCD predictions and the data were effectively decreased by the inclusion of the partial NLO contributions, the central values of the pQCD predictions for  $Br(B \rightarrow K\eta')$  are still lower than the data by about 30%. As for the CP-violating asymmetries, the pQCD predictions in Ref. [12] already agree well with the data.

Very recently, three new advances in the studies of the two-body charmless hadronic  $B \rightarrow M_2 M_3$  decays (here  $M_i$  stands for the light mesons, such as  $\pi, K, \eta^{(\prime)}$ , etc.) in the pQCD factorization approach have been made:

- (i) In Ref. [14], Li et al. calculated the NLO contributions to the form factors of  $B \rightarrow \pi$  transitions in the pQCD approach and found that the NLO part can provide a roughly 20% enhancement to the LO one. The enhanced form factors may then lead to a larger branching ratio for  $B \rightarrow K\eta'$  decays. The still missing NLO parts in the pQCD approach are the  $O(\alpha_s^2)$  contributions from nonfactorizable spectator diagrams and the annihilation diagrams, which are most likely small according to general arguments.

- (ii) In Ref. [15], the authors studied and provided a successful pQCD interpretation for the Belle measurements of  $B_d/B_s \rightarrow J/\Psi\eta^{(\prime)}$ , i.e.,  $R_q^{exp} = Br(B_q \rightarrow J/\Psi\eta^{(\prime)})/Br(B_q \rightarrow J/\Psi\eta) < 1$  with  $q = (d, s)$ , by using the  $\eta$ - $\eta'$ - $G$  mixing formalism[16], where  $G$  represents the pseudoscalar glueball. This result encourages us to check the possible effects of the pseudoscalar  $G$  on  $B \rightarrow K\eta^{(\prime)}$  decays, although such contributions may be small as generally expected [17].
- (iii) In Ref. [18], the authors studied the  $\eta$ - $\eta'$ - $G$ - $\eta_c$  mixing scheme, obtained constraints on the mixing angle  $\phi_Q$  ( $\phi_Q \sim 11^\circ$ ) between  $G$  and  $\eta_c$  by fitting to the observed  $\eta_c$  decay widths and other relevant data, and found that the  $\eta_c$  mixing can enhance the pQCD predictions for  $Br(B \rightarrow K\eta')$  by 18%, but does not alter those for  $Br(B \rightarrow K\eta)$ . In Ref. [18], the authors superposed the contributions from  $B \rightarrow K\eta_c$  due to the  $\eta_c$  mixing onto the partial NLO pQCD predictions as given in Ref. [12] directly. They did not consider the effects of the newly known NLO contributions to the corresponding form factors  $F_0^{B \rightarrow K}(0)$  and  $F_0^{B \rightarrow \eta^{(\prime)}}(0)$ .

Motivated by the above new advances[14, 15, 18], we think that it is time for us to make a comprehensive study of the four  $B \rightarrow K\eta^{(\prime)}$  decays in the pQCD factorization approach. We will focus on the following points:

- (i) Besides those NLO contributions already considered in Ref. [12], we here will firstly extend the calculation of the NLO part of the form factors for the  $B \rightarrow \pi$  transition [14] to the cases for the similar  $B \rightarrow K$  and  $B \rightarrow (\eta_q, \eta_s)$  transitions, and then take these newly known form factors at the NLO level into the calculations for the branching ratios and CP-violating asymmetries of  $B \rightarrow K\eta^{(\prime)}$  decays, to check its effects on the corresponding pQCD predictions.
- (ii) Besides the ordinary FKS  $\eta$ - $\eta'$  mixing scheme [13], we will also calculate these four decays in the  $\eta$ - $\eta'$ - $G$  [16] mixing scheme and the  $\eta$ - $\eta'$ - $G$ - $\eta_c$  mixing scheme [18], respectively. We want to check the effects of the possible "pseudoscalar glueball" and  $\eta_c$  component of the  $\eta^{(\prime)}$  meson on the pQCD predictions.
- (iii) We will numerically calculate the individual decay amplitudes  $\mathcal{M}^{a+b}$  [ the emission diagrams Figs.1(a) and 1(b)],  $\mathcal{M}^{c+d}$  [the spectator diagrams Figs.1(c) and 1(d)] and  $\mathcal{M}^{anni}$  [annihilation diagrams Figs.1(e)-1(h) ] and compare the relative strength of the contributions from different sets of the Feynman diagrams at the leading order, or from the different sources at the next-to-leading order, such as  $\mathcal{M}_{VC}$  (i.e. NLO vertex corrections Figs.3(a)-3(d) ),  $\mathcal{M}_{ql}$  [ i.e., NLO quark-loops Figs.3(e) and 3(f)], and  $\mathcal{M}_{mp}$  [ i.e., NLO chromomagnetic penguins Figs.3(g) and 3(h)]. We try to find the source of the dominant contribution, in order to estimate the possible strength of the two still missing NLO contributions in the pQCD approach.

The paper is organized as follows. In Sec. II, we give a brief discussion of the pQCD factorization approach and the three different kinds of mixing schemes:  $\eta$ - $\eta'$ ,  $\eta$ - $\eta'$ - $G$ , and  $\eta$ - $\eta'$ - $G$ - $\eta_c$  mixing schemes. In Sec. III, we make the analytic calculations of the relevant Feynman diagrams and present the various decay amplitudes for the studied decay modes in leading order. In Sec. IV, all currently known NLO contributions in the pQCD approach are investigated. In Sec. V, we will show the numerical results for the pQCD predictions for the branching ratios and CP-violating asymmetries of the considered decay modes,

and calculate and compare the relative strength of the LO and NLO contributions from different sets of the Feynman diagrams or from different sources. The summary and some discussions are included in the final section.

## II. THEORETICAL FRAMEWORK

As is well known, the pQCD factorization approach has been widely used in studies for the two-body charmless hadronic  $B/B_s/B_c \rightarrow M_2 M_3$  decays (here  $M_i$  stands for the light pseudoscalar meson  $P$ , the vector meson  $V$ , the scalar meson  $S$ , etc.) [5, 8, 9, 12, 14, 19–25]. Some pQCD predictions—for example, the large CP-violating asymmetries  $\mathcal{A}_{CP}^{dir}(B^0 \rightarrow \pi^+ \pi^-) \approx (30 \pm 10)\%$  in Ref. [6] and the large branching ratio  $Br(B_s \rightarrow \pi^+ \pi^-) \approx 5 \times 10^{-6}$  in Refs. [20, 26], -have been confirmed by experiments[25]. We here focus on the study of the four  $B \rightarrow K \eta^{(\prime)}$  decays. For more details of the formalism of the pQCD factorization approach itself, one can see, for example, Refs. [9, 12, 21, 27].

### A. Outline of $B \rightarrow K \eta^{(\prime)}$ decays in the pQCD approach

In the B rest frame, we assume that the light final-state meson  $M_2$  and  $M_3$  is moving along the direction of  $n = (1, 0, \mathbf{0}_T)$  and  $v = (0, 1, \mathbf{0}_T)$ , respectively. We use  $x_i$  to denote the momentum fraction of the antiquark in each meson, and  $k_{i\perp}$  the corresponding transverse momentum. Using the light-cone coordinates the  $B$ -meson momentum  $P_B$  and the two final-state meson's momenta  $P_2$  and  $P_3$  (for  $M_2$  and  $M_3$  respectively) can be written as

$$P_B = \frac{M_B}{\sqrt{2}}(1, 1, \mathbf{0}_T), \quad P_2 = \frac{M_B}{\sqrt{2}}(1 - r_3^2, r_2^2, \mathbf{0}_T), \quad P_3 = \frac{M_B}{\sqrt{2}}(r_3^2, 1 - r_2^2, \mathbf{0}_T), \quad (3)$$

where  $r_i = m_i/M_B$  with  $m_i$  being the mass of meson  $M_i$ . If we choose

$$\begin{aligned} k_1 &= \frac{m_B}{\sqrt{2}}(x_1, 0, \mathbf{k}_{1T}), \quad k_2 = \frac{m_B}{\sqrt{2}}(x_2(1 - r_3^2), x_2 r_2^2, \mathbf{k}_{2T}), \\ k_3 &= \frac{m_B}{\sqrt{2}}(x_3 r_3^2, x_3(1 - r_2^2), \mathbf{k}_{3T}), \end{aligned} \quad (4)$$

The integration over the small components  $k_1^-, k_2^-$ , and  $k_3^+$  will lead conceptually to the decay amplitudes,

$$\begin{aligned} \mathcal{A}(B \rightarrow M_2 M_3) &\sim \int dx_1 dx_2 dx_3 b_1 db_1 b_2 db_2 b_3 db_3 \\ &\cdot \text{Tr} [C(t) \Phi_B(x_1, b_1) \Phi_{M_2}(x_2, b_2) \Phi_{M_3}(x_3, b_3) H(x_i, b_i, t) S_t(x_i) e^{-S(t)}], \end{aligned} \quad (5)$$

where  $b_i$  is the conjugate space coordinate of  $k_{iT}$ . In the above equation,  $C(t)$  is the Wilson coefficient evaluated at scale  $t$ , which includes the large logarithms ( $\ln m_W/t$ ) coming from QCD radiative corrections to four-quark operators. The functions  $\Phi_B(x_1, b_1)$ ,  $\Phi_{M_2}(x_2, b_2)$ , and  $\Phi_{M_3}(x_3, b_3)$  are the wave functions of the initial B meson and the final-state meson  $M_2$  and  $M_3$  respectively. These wave functions describe the hadronization of the quark and antiquark in the meson  $B$  and  $M_{2,3}$ . The “hard kernel”  $H(k_1, k_2, k_3, t)$  describes the

four-quark operator and the spectator quark connected by a hard gluon whose  $q^2$  is in the order of  $\bar{\Lambda}M_B$ , and includes the  $\mathcal{O}(\sqrt{\bar{\Lambda}M_B})$  hard dynamics.

The jet function  $S_t(x_i)$  in Eq.(5)—as given explicitly in Eq.(B7) of Appendix B— is one of the two kinds of Sudakov form factors relevant for the B decays considered, which come from the threshold resummation over the large double logarithms  $(\ln^2 x_i)$  in the end-point region. This jet function  $S_t(x_i)$  vanishes as  $x_i \rightarrow 0, 1$ , and smears the end-point singularities on  $x_i$  for meson distribution amplitudes.

Similarly, the inclusion of  $k_T$  regulates the end-point singularities. The large double logarithms  $\alpha_s \ln^2 k_T$  should also be organized to all orders, leading to a  $k_T$  resummation [28]. The resultant Sudakov form factors  $S_B(t)$ ,  $S_2(t)$  and  $S_3(t)$  for the B meson and two final-state mesons  $M_{2,3}$ — whose explicit expressions can be found in Eq.(B9) of Appendix B — keep the magnitude of  $k_T^2$  to be at roughly  $\mathcal{O}(\bar{\Lambda}m_B)$  by suppressing the region with  $k_T^2 \sim \mathcal{O}(\bar{\Lambda}^2)$ . The exponential function  $e^{-S(t)}$  in Eq.(5)— where  $s(t) = S_B(t) + S_2(t) + S_3(t)$  or  $S(t) = S_B(t) + S_i(t)$  with  $i = 2$  or  $3$  as shown in Eq.(B8) of Appendix B — is also called the Sudakov form factor, which effectively suppresses the soft dynamics at the end-point region [9]. Of course, more studies are required to check the actual suppression effect on possible nonperturbative contributions due to the introduction of the Sudakov form factors. Some theoretical errors may also be produced due to the uncertainties of  $S_t(x_i)$  and  $e^{-S(t)}$ .

For the studied  $B \rightarrow K\eta^{(\prime)}$  decays, the corresponding weak effective Hamiltonian can be written as [29]

$$\mathcal{H}_{eff} = \frac{G_F}{\sqrt{2}} \left\{ V_{ub}V_{uq}^* \left[ C_1(\mu)O_1^u(\mu) + C_2(\mu)O_2^u(\mu) \right] - V_{tb}V_{tq}^* \left[ \sum_{i=3}^{10} C_i(\mu)O_i(\mu) \right] \right\} + \text{H.c.}, \quad (6)$$

where  $q = d, s$ ,  $G_F = 1.16639 \times 10^{-5} \text{GeV}^{-2}$  is the Fermi constant. The  $O_i$  ( $i = 1, \dots, 10$ ) are the local four-quark operators,

$$O_1^u = (\bar{u}_\alpha b_\beta)_{V-A} (\bar{q}_\beta u_\alpha)_{V-A}, \quad O_2^u = (\bar{u}_\alpha b_\alpha)_{V-A} (\bar{q}_\beta u_\beta)_{V-A}, \quad (7)$$

$$O_3 = (\bar{q}_\alpha b_\alpha)_{V-A} \sum_{q'} (\bar{q}'_\beta q'_\beta)_{V-A}, \quad O_4 = (\bar{q}_\beta b_\alpha)_{V-A} \sum_{q'} (\bar{q}'_\alpha q'_\beta)_{V-A},$$

$$O_5 = (\bar{q}_\alpha b_\alpha)_{V-A} \sum_{q'} (\bar{q}'_\beta q'_\beta)_{V+A}, \quad O_6 = (\bar{q}_\beta b_\alpha)_{V-A} \sum_{q'} (\bar{q}'_\alpha q'_\beta)_{V+A}, \quad (8)$$

$$O_7 = \frac{3}{2} (\bar{q}_\alpha b_\alpha)_{V-A} \sum_{q'} e_{q'} (\bar{q}'_\beta q'_\beta)_{V+A}, \quad O_8 = \frac{3}{2} (\bar{q}_\beta b_\alpha)_{V-A} \sum_{q'} e_{q'} (\bar{q}'_\alpha q'_\beta)_{V+A},$$

$$O_9 = \frac{3}{2} (\bar{q}_\alpha b_\alpha)_{V-A} \sum_{q'} e_{q'} (\bar{q}'_\beta q'_\beta)_{V-A}, \quad O_{10} = \frac{3}{2} (\bar{q}_\beta b_\alpha)_{V-A} \sum_{q'} e_{q'} (\bar{q}'_\alpha q'_\beta)_{V-A}, \quad (9)$$

where  $\alpha$  and  $\beta$  are the color indices and  $q'$  are the active quarks at the scale  $m_b$ , i.e.  $q' = (u, d, s, c, b)$ . The left-handed current is defined as  $(\bar{q}_\alpha q_\beta)_{V-A} = \bar{q}_\alpha \gamma_\nu (1 - \gamma_5) q_\beta$  and the right-handed current  $(\bar{q}_\alpha q_\beta)_{V+A} = \bar{q}_\alpha \gamma_\nu (1 + \gamma_5) q_\beta$ .

In this paper, we will calculate  $B \rightarrow K\eta^{(\prime)}$  decays in the pQCD approach with the inclusion of all known NLO contributions, and focus on the effects of the newly known NLO contributions to the form factors  $F_0^{B \rightarrow K}(0)$  and  $F_0^{B \rightarrow \eta^{(\prime)}}(0)$  [14].

## B. Different mixing schemes

Both  $\eta$  and  $\eta'$  mesons – according to currently available studies [13, 16, 18, 30] – may contain a small gluonic component (an  $\eta_c$  or even a  $\pi^0$  component) through mixing.

In order to check the mixing-scheme dependence of the pQCD predictions for the physical observables of the considered decays we will calculate the  $B \rightarrow K\eta^{(\prime)}$  decays in the following three typical mixing schemes(MS):

- (i) MS-1: The FKS scheme [13] of  $\eta$ - $\eta'$  mixing in the quark-flavor basis <sup>1</sup>:  $\eta_q = (u\bar{u} + d\bar{d})/\sqrt{2}$  and  $\eta_s = s\bar{s}$ .
- (ii) MS-2: The  $\eta$ - $\eta'$ - $G$  mixing scheme as defined in Ref. [16].
- (iii) MS-3: The  $\eta$ - $\eta'$ - $G$ - $\eta_c$  mixing scheme as defined in Ref. [18].

Firstly, in the FKS  $\eta$ - $\eta'$  mixing scheme in the quark-flavor basis, the physical  $\eta$  and  $\eta'$  can be written as

$$\begin{pmatrix} \eta \\ \eta' \end{pmatrix} = U(\phi) \begin{pmatrix} \eta_q \\ \eta_s \end{pmatrix} = \begin{pmatrix} \cos \phi & -\sin \phi \\ \sin \phi & \cos \phi \end{pmatrix} \begin{pmatrix} \eta_q \\ \eta_s \end{pmatrix}, \quad (10)$$

where  $\phi$  is the mixing angle. The relation between the decay constants ( $f_\eta^q, f_\eta^s, f_{\eta'}^q, f_{\eta'}^s$ ) and ( $f_q, f_s$ ) can be found in Refs. [12, 13]. The chiral enhancements  $m_0^q$  and  $m_0^s$  have been defined in Ref. [21] by assuming the exact isospin symmetry  $m_q = m_u = m_d$ . The three input parameters  $f_q, f_s$ , and  $\phi$  in the FKS mixing scheme have been extracted from the data of the relevant exclusive processes [13]

$$f_q = (1.07 \pm 0.02)f_\pi, \quad f_s = (1.34 \pm 0.06)f_\pi, \quad \phi = 39.3^\circ \pm 1.0^\circ. \quad (11)$$

With  $f_\pi = 0.13$  GeV, the chiral enhancements  $m_0^q$  and  $m_0^s$  consequently take the values of  $m_0^q = 1.07$  GeV and  $m_0^s = 1.92$  GeV [21].

In Ref. [16], the authors extended the conventional FKS mixing scheme to include the possible pseudoscalar glueball  $G$ , i.e., a small gluonic component in both  $\eta$  and  $\eta'$  mesons [30]. In their  $\eta$ - $\eta'$ - $G$  mixing scheme, the physical states ( $\eta, \eta', G$ ) are related to  $(\eta_8, \eta_1, g)$  and  $(\eta_q, \eta_s, g)$  through the rotation  $U(\phi, \phi_G) = U_3(\theta)U_1(\phi_G)U_3(\theta_i)$ [16],

$$\begin{pmatrix} |\eta\rangle \\ |\eta'\rangle \\ |G\rangle \end{pmatrix} = U_3(\theta)U_1(\phi_G) \begin{pmatrix} |\eta_8\rangle \\ |\eta_1\rangle \\ |g\rangle \end{pmatrix} = U_3(\theta)U_1(\phi_G)U_3(\theta_i) \begin{pmatrix} |\eta_q\rangle \\ |\eta_s\rangle \\ |g\rangle \end{pmatrix}, \quad (12)$$

with the rotation matrices [16]

$$U_3(\theta) = \begin{pmatrix} \cos \theta & -\sin \theta & 0 \\ \sin \theta & \cos \theta & 0 \\ 0 & 0 & 1 \end{pmatrix}, \quad U_1(\phi_G) = \begin{pmatrix} 1 & 0 & 0 \\ 0 & \cos \phi_G & \sin \phi_G \\ 0 & -\sin \phi_G & \cos \phi_G \end{pmatrix},$$

$$U(\phi, \phi_G) = \begin{pmatrix} \cos \phi + \sin \theta \sin \theta_i \Delta_G & -\sin \phi + \sin \theta \cos \theta_i \Delta_G & -\sin \theta \sin \phi_G \\ \sin \phi - \cos \theta \sin \theta_i \Delta_G & \cos \phi - \cos \theta \cos \theta_i \Delta_G & \cos \theta \sin \phi_G \\ -\sin \theta_i \sin \phi_G & -\cos \theta_i \sin \phi_G & \cos \phi_G \end{pmatrix}, \quad (13)$$

---

<sup>1</sup> In the octet-singlet basis, one assumes  $\eta_1 = (\bar{u}u + \bar{d}d + \bar{s}s)/\sqrt{3}$  and  $\eta_8 = (\bar{u}u + \bar{d}d - 2\bar{s}s)/\sqrt{6}$ .

where  $\theta_i = 54.7^\circ$  is the ideal mixing angle with  $\cos \theta_i = 1/\sqrt{3}$  and  $\sin \theta_i = \sqrt{2/3}$ , the angle  $\phi = \theta + \theta_i$  and the abbreviation  $\Delta G = 1 - \cos \phi_G$ . One can see that the matrix  $U(\phi, \phi_G)$  will approach the FKS mixing matrix [13] in the limit of  $\phi_G \rightarrow 0$ , which means that the angle  $\phi$  in Eq. (13) plays the same role as the mixing angle in the FKS mixing scheme[16].

The chiral masses  $m_0^q$  and  $m_0^s$  in the  $\eta$ - $\eta'$ - $G$  mixing scheme can be written as [16]

$$m_0^q = \frac{m_{qq}^2}{2m_q} = \frac{1}{2m_q} (U_{11} - \frac{\sqrt{2}f_s}{f_q} U_{12}), \quad (14)$$

$$m_0^s = \frac{m_{ss}^2}{2m_s} = \frac{1}{2m_s} (U_{22} - \frac{f_q}{\sqrt{2}f_s} U_{21}), \quad (15)$$

with the rotation matrix elements  $U_{ij}$  having the form [16]

$$\begin{aligned} U_{11} &= (\cos \phi + \sin \theta \sin \theta_i \Delta_G)^2 m_\eta^2 + (\sin \phi - \cos \theta \sin \theta_i \Delta_G)^2 m_{\eta'}^2 + (\sin \theta_i \sin \phi_G)^2 m_G^2, \\ U_{12} &= U_{21} = (\cos \phi + \sin \theta \sin \theta_i \Delta_G) \cdot (-\sin \phi + \sin \theta \cos \theta_i \Delta_G) m_\eta^2 \\ &\quad + (\sin \phi - \cos \theta \sin \theta_i \Delta_G) \cdot (\cos \phi - \cos \theta \cos \theta_i \Delta_G) m_{\eta'}^2 + \sin \theta_i \sin \phi_G \cdot \cos \theta_i \sin \phi_G m_G^2, \\ U_{22} &= (-\sin \phi + \sin \theta \cos \theta_i \Delta_G)^2 m_\eta^2 + (\cos \phi - \cos \theta \cos \theta_i \Delta_G)^2 m_{\eta'}^2 \\ &\quad + (\cos \theta_i \sin \phi_G)^2 m_G^2. \end{aligned} \quad (16)$$

The decay constants associated with the physical  $(\eta, \eta', G)$  states are related to those associated with  $(\eta_q, \eta_s, g)$  states via the same mixing matrix[16]

$$\begin{pmatrix} f_\eta^q & f_\eta^s \\ f_{\eta'}^q & f_{\eta'}^s \\ f_G^q & f_G^s \end{pmatrix} = U(\phi, \phi_G) \begin{pmatrix} f_q & f_q^s \\ f_s^q & f_s^s \\ f_g^q & f_g^s \end{pmatrix}. \quad (17)$$

The mixing angle  $\phi_G$  describes the mixing between the flavor singlet  $\eta_1$  and unmixed glueball  $g$  and can vary in a range, depending on the parametrization of the mixing matrix, experimental inputs, and the fitting procedure. Since current data and known theoretical estimations [17] suggest a rather small gluonic component in  $\eta^{(l)}$ , the angle  $\phi_G$  should be small as well. Following Ref. [16], we also take  $\phi_G = 12^\circ$ .

For the mass of the pseudoscalar glueball, the theoretical prediction for  $m_G$  depends on the choice of input parameters, such as  $(m_\eta, m_{\eta'}, f_s, f_q, \text{etc})$ . The theoretical estimations in Refs. [16, 18] prefer a value of  $m_G \approx 1.3 - 1.5$  GeV. If we take  $f_q = f_\pi$  and  $f_s = 1.3f_\pi$  in the numerical estimations, we find that  $m_G = 1.376$  GeV ( see Table I of Ref. [18] ) from the approximate correlation relation between  $m_G$  and the other input parameters as given in Eq.(35) of Ref. [18]. For other input parameters we also follow the choice of Refs. [16, 18], and finally we take

$$f_q = f_\pi, \quad f_s = 1.3f_\pi, \quad \phi = 43.7^\circ \quad \phi_G = 12^\circ, \quad m_G = 1.376 \text{ GeV}, \quad (18)$$

in the numerical calculations when the  $\eta$ - $\eta'$ - $G$  scheme is adopted.

In the third  $\eta$ - $\eta'$ - $G$ - $\eta_c$  mixing scheme[18], finally, the flavor states are transformed into the physical states through the mixing matrix  $U(\theta, \phi_G, \phi_Q)$ :

$$\begin{pmatrix} |\eta\rangle \\ |\eta'\rangle \\ |G\rangle \\ |\eta_c\rangle \end{pmatrix} = U(\theta, \phi_G, \phi_Q) \begin{pmatrix} |\eta_q\rangle \\ |\eta_s\rangle \\ |g\rangle \\ |\eta_Q\rangle \end{pmatrix}, \quad (19)$$

with the  $4 \times 4$  mixing matrix [18]

$$U(\theta, \phi_G, \phi_Q) = \begin{pmatrix} c\theta c\theta_i - s\theta c\phi_G s\theta_i & -c\theta s\theta_i - s\theta c\phi_G c\theta_i & -s\theta s\phi_G c\phi_Q & -s\theta s\phi_G s\phi_Q \\ s\theta c\theta_i + c\theta c\phi_G s\theta_i & -s\theta s\theta_i + c\theta c\phi_G c\theta_i & c\theta s\phi_G c\phi_Q & c\theta s\phi_G s\phi_Q \\ -s\phi_G s\theta_i & -s\phi_G c\theta_i & c\phi_G c\phi_Q & c\phi_G s\phi_Q \\ 0 & 0 & -s\phi_Q & c\phi_Q \end{pmatrix} \quad (20)$$

where  $\theta_i = 54.7^\circ$  is the ideal mixing angle,  $\theta = \phi - \theta_i$  (here  $\phi$  is the previous mixing angle in the FKS mixing scheme), and  $c\theta$  ( $s\theta$ ) is the abbreviation for  $\cos\theta$  ( $\sin\theta$ ) and similarly for others. With the definition of  $\phi = \theta + \theta_i$ , the rotation matrix  $U(\theta, \phi_G, \phi_Q)$  in Eq. (20) approaches the mixing matrix  $U(\phi, \phi_G)$  in Eq. (13) in the  $\phi_Q \rightarrow 0$  limit, or the FKS mixing matrix  $U(\phi)$  [13] in the limits of  $\phi_Q \rightarrow 0$  and  $\phi_G \rightarrow 0$ .

The decay constants associated with the  $\eta$ ,  $\eta'$ ,  $G$ , and  $\eta_c$  physical states are related to those associated with the  $\eta_q$ ,  $\eta_s$ ,  $g$ ,  $\eta_Q$  states through the mixing matrix  $U(\theta, \phi_G, \phi_Q)$ :

$$\begin{pmatrix} f_\eta^q & f_\eta^s & f_\eta^c \\ f_{\eta'}^q & f_{\eta'}^s & f_{\eta'}^c \\ f_G^q & f_G^s & f_G^c \\ f_{\eta_c}^q & f_{\eta_c}^s & f_{\eta_c}^c \end{pmatrix} = U(\theta, \phi_G, \phi_Q) \begin{pmatrix} f_q & f_q^s & f_q^c \\ f_s^q & f_s^s & f_s^c \\ f_g^q & f_g^s & f_g^c \\ f_c^q & f_c^s & f_c^c \end{pmatrix}. \quad (21)$$

Furthermore, we find that the chiral masses  $m_0^q$  and  $m_0^s$  in this mixing scheme are identical to those as given in Eqs. (14) and (15). In the  $\eta$ - $\eta'$ - $G$ - $\eta_c$  mixing scheme, we also take  $\phi_Q = 11^\circ$  as per Ref. [18], while we choose the other input parameters to be the same as those given in Eq. (18), i.e.,

$$f_q = f_\pi, \quad f_s = 1.3f_\pi, \quad \theta = -11^\circ, \quad \phi_G = 12^\circ, \quad \phi_Q = 11^\circ, \quad m_G = 1.376 \text{ GeV}, \quad (22)$$

### C. Wave functions

The  $B$  meson is treated as a very good heavy-light system. Its wave function can be written as the form of

$$\Phi_B = \frac{i}{\sqrt{2N_c}} (\not{P}_B + m_B) \gamma_5 \phi_B(\mathbf{k}_1). \quad (23)$$

Here we have adopted the B-meson distribution amplitude  $\phi_B(x, b)$  widely used in the studies of B-meson hadronic decays based on the pQCD factorization approach since 2001 [4–6, 9, 31, 32]

$$\phi_B(x, b) = N_B x^2 (1-x)^2 \exp \left[ -\frac{M_B^2 x^2}{2\omega_b^2} - \frac{1}{2}(\omega_b b)^2 \right], \quad (24)$$

where the  $b$ -dependence was included through the second term in the exponential function, the shape parameter  $\omega_b = 0.40 \pm 0.04$  has been fixed [9] from the fit to the  $B \rightarrow \pi$  form factors derived from lattice QCD [33] and from the light-cone sum rule [34] and finally the normalization factor  $N_B$  depends on the values of  $\omega_b$  and  $f_B$  and defined through the normalization relation

$$\int_0^1 dx \phi_B(x, b=0) = \frac{f_B}{2\sqrt{6}}. \quad (25)$$



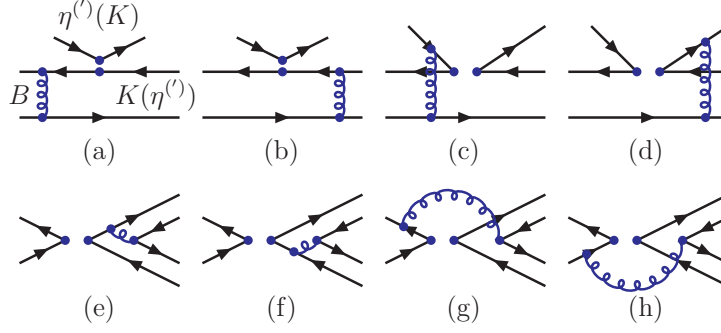


FIG. 1. Feynman diagrams that may contribute to the  $B \rightarrow K\eta^{(\prime)}$  decays in the pQCD approach at leading order.

The wave functions of the final-state mesons  $M = (K, \eta_q, \eta_s)$  are defined as:

$$\Phi_{M_i}(P_i, x_i) \equiv \frac{i}{\sqrt{2N_C}} \gamma_5 [\not{P}_i \phi_{M_i}^A(x_i) + m_{0i} \phi_{M_i}^P(x_i) + m_{0i} (\not{\epsilon} \not{P}_i - 1) \phi_{M_i}^T(x_i)], \quad (26)$$

where  $m_{0i}$  is the corresponding meson chiral mass, and  $P_i$  and  $x_i$  are the momentum and the momentum fraction of  $M_i$ , respectively. The explicit expressions of the distribution amplitudes  $\phi_{M_i}^{A,P,T}(x_i)$  for  $M = (K, \eta_q, \eta_s)$  are given in Appendix A.

In the third  $\eta$ - $\eta'$ - $G$ - $\eta_c$  mixing scheme, the  $\eta_c$  part of the  $\eta^{(\prime)}$  meson will contribute to the  $B \rightarrow K\eta^{(\prime)}$  decays through the decay chain  $B \rightarrow K\eta_c \rightarrow K\eta^{(\prime)}$ . The wave function of the  $\eta_c$  can be written as[35]:

$$\Phi_{\eta_c}(P_2, x_2) \equiv \frac{i}{\sqrt{2N_C}} \gamma_5 [\not{P}_2 \phi_{\eta_c}^\nu(x_2) + m_{\eta_c} \phi_{\eta_c}^s(x_2)]. \quad (27)$$

The distribution amplitudes  $\phi_{\eta_c}^{\nu,s}$  are of the form [35]:

$$\begin{aligned} \phi_{\eta_c}^\nu(x) &= 9.58 \frac{f_{\eta_c}}{2\sqrt{2N_c}} x(1-x) \left[ \frac{x(1-x)}{1-2.8x(1-x)} \right]^{0.7}, \\ \phi_{\eta_c}^s(x) &= 1.97 \frac{f_{\eta_c}}{2\sqrt{2N_c}} \left[ \frac{x(1-x)}{1-2.8x(1-x)} \right]^{0.7}. \end{aligned} \quad (28)$$

### III. $B \rightarrow K\eta^{(\prime)}$ AND $B \rightarrow K\eta_c$ DECAYS AT LEADING ORDER

In this section we will present the total decay amplitudes for  $B \rightarrow K\eta^{(\prime)}$  and  $B \rightarrow K\eta_c$  decays in the pQCD approach at leading order.

#### A. $B \rightarrow K\eta^{(\prime)}$ decays at leading order

The  $B \rightarrow K\eta^{(\prime)}$  decays have been studied by using the ordinary  $\eta$ - $\eta'$  mixing scheme and by employing the pQCD factorization approach at the LO and partial NLO level

in Ref. [12]. We recalculated and confirmed the relevant analytical formulas as given in Ref. [12]. For the sake of the reader, we here present directly the decay amplitudes obtained by evaluating the Feynman diagrams Figs.1(a)-1(h).

For the factorizable emission diagrams Figs.1(a) and 1(b), the decay amplitudes for the cases of a  $B \rightarrow K$  transition are of the form

$$F_{eK}^{V-A} = -F_{eK}^{V+A} = -8\pi C_F M_B^4 \int_0^1 dx_1 dx_3 \int_0^\infty b_1 db_1 b_3 db_3 \phi_B(x_1, b_1) \times \left\{ \left[ (1+x_3)\phi_K^A(x_3) + r_3(1-2x_3)(\phi_K^P(x_3) + \phi_K^T(x_3)) \right] \times E_e(t_a) h_e(x_1, x_3, b_1, b_3) + 2r_3\phi_K^P(x_3) E_e(t'_a) h_e(x_3, x_1, b_3, b_1) \right\}, \quad (29)$$

$$F_{eK}^{SP} = -16\pi r_2 C_F M_B^4 \int_0^1 dx_1 dx_3 \int_0^\infty b_1 db_1 b_3 db_3 \phi_B(x_1, b_1) \times \left\{ \left[ \phi_K^A(x_3) + r_3(2+x_3)\phi_K^P(x_3) - r_3 x_3 \phi_K^T(x_3) \right] \times E_e(t_a) h_e(x_1, x_3, b_1, b_3) + 2r_3\phi_K^P(x_3) E_e(t'_a) h_e(x_3, x_1, b_3, b_1) \right\}, \quad (30)$$

where  $C_F = 4/3$ ,  $r_2 = r_\eta = m_0^{q,s}/M_B$ , and  $r_3 = r_K = m_0^K/M_B$ . The hard functions,  $E_e(t)$  and  $h_e$ , and the hard scales  $t$  are given in Appendix B.

For the non-factorizable emission diagrams Figs.1(c) and 1(d), whose contributions are

$$M_{eK}^{V-A} = -\frac{32\pi C_F M_B^4}{\sqrt{6}} \int_0^1 dx_1 dx_2 dx_3 \int_0^\infty b_1 db_1 b_2 db_2 \phi_B(x_1, b_1) \phi_\eta^A(x_2) \times \left\{ \left[ (1-x_2)\phi_K^A(x_3) - r_3 x_3 (\phi_K^P(x_3) - \phi_K^T(x_3)) \right] E'_e(t_b) h_n(x_1, \bar{x}_2, x_3, b_1, b_2) + \left[ - (x_2 + x_3)\phi_K^A(x_3) + r_3 x_3 (\phi_K^P(x_3) + \phi_K^T(x_3)) \right] \times E'_e(t'_b) h_n(x_1, x_2, x_3, b_1, b_2) \right\}, \quad (31)$$

$$M_{eK}^{V+A} = -\frac{32\pi C_F M_B^4 r_2}{\sqrt{6}} \int_0^1 dx_1 dx_2 dx_3 \int_0^\infty b_1 db_1 b_2 db_2 \phi_B(x_1, b_1) \times \left\{ \left[ (1-x_2)\phi_K^A(x_3) (\phi_\eta^P(x_2) + \phi_\eta^T(x_2)) + r_3 x_3 (\phi_\eta^P(x_2) - \phi_\eta^T(x_2)) (\phi_K^P(x_3) + \phi_K^T(x_3)) + (1-x_2)r_3 (\phi_2^P(x_2) + \phi_2^T(x_2)) (\phi_3^P(x_3) - \phi_3^T(x_3)) \right] E'_e(t_b) h_n(x_1, \bar{x}_2, x_3, b_1, b_2) - \left[ x_2\phi_K^A(x_3) (\phi_\eta^P(x_2) - \phi_\eta^T(x_2)) + r_3 x_2 (\phi_\eta^P(x_2) - \phi_\eta^T(x_2)) (\phi_K^P(x_3) - \phi_K^T(x_3)) + r_3 x_3 (\phi_\eta^P(x_2) + \phi_\eta^T(x_2)) (\phi_K^P(x_3) + \phi_K^T(x_3)) \right] \cdot E'_e(t'_b) h_n(x_1, x_2, x_3, b_1, b_2) \right\}, \quad (32)$$

$$M_{eK}^{SP} = -\frac{32\pi C_F M_B^4}{\sqrt{6}} \int_0^1 dx_1 dx_2 dx_3 \int_0^\infty b_1 db_1 b_2 db_2 \phi_B(x_1, b_1) \phi_\eta^A(x_2) \times \left\{ \left[ (x_2 - x_3 - 1)\phi_K^A(x_3) + r_3 x_3 (\phi_K^P(x_3) + \phi_K^T(x_3)) \right] E'_e(t_b) h_n(x_1, \bar{x}_2, x_3, b_1, b_2) + \left[ x_2\phi_K^A(x_3) + r_3 x_3 (\phi_K^T(x_3) - \phi_K^P(x_3)) \right] E'_e(t'_b) h_n(x_1, x_2, x_3, b_1, b_2) \right\}, \quad (33)$$

where  $\bar{x}_i = 1 - x_i$ , while  $\phi_\eta$  denotes  $\phi_{\eta_q}$  or  $\phi_{\eta_s}$ .

For the factorizable annihilation diagrams Figs.1(e) and 1(f), the decay amplitudes are of the form

$$\begin{aligned}
F_{aK}^{V-A} = F_{aK}^{V+A} = & -8\pi C_F M_B^4 \int_0^1 dx_2 dx_3 \int_0^\infty b_2 db_2 b_3 db_3 \times \left\{ \left[ (x_3 - 1) \phi_\eta^A(x_2) \phi_K^A(x_3) \right. \right. \\
& - 4r_2 r_3 \phi_\eta^P(x_2) \phi_K^P(x_3) + 2r_2 r_3 x_3 \phi_\eta^P(x_2) (\phi_K^P(x_3) - \phi_K^T(x_3)) \left. \right] E_a(t_c) h_a(x_2, \bar{x}_3, b_2, b_3) \\
& + \left[ x_2 \phi_\eta^A(x_2) \phi_K^A(x_3) + 2r_2 r_3 (\phi_\eta^P(x_2) - \phi_\eta^T(x_2)) \phi_K^P(x_3) \right. \\
& \left. \left. + 2r_2 r_3 x_2 (\phi_\eta^P(x_2) + \phi_\eta^T(x_2)) \phi_K^P(x_3) \right] E_a(t'_c) h_a(\bar{x}_3, x_2, b_3, b_2) \right\}, \quad (34)
\end{aligned}$$

$$\begin{aligned}
F_{aK}^{SP} = & -16\pi C_F M_B^4 \int_0^1 dx_2 dx_3 \int_0^\infty b_2 db_2 b_3 db_3 \\
& \times \left\{ \left[ 2r_2 \phi_\eta^P(x_2) \phi_K^A(x_3) + (1 - x_3) r_3 \phi_\eta^A(x_2) (\phi_K^P(x_3) + \phi_K^T(x_3)) \right] E_a(t_c) h_a(x_2, \bar{x}_3, b_2, b_3) \right. \\
& \left. + \left[ 2r_3 \phi_\eta^A(x_2) \phi_K^P(x_3) + r_2 x_2 (\phi_\eta^P(x_2) - \phi_\eta^T(x_2)) \phi_K^A(x_3) \right] E_a(t'_c) h_a(\bar{x}_3, x_2, b_3, b_2) \right\}. \quad (35)
\end{aligned}$$

The contributions from the non-factorizable annihilation diagrams, Figs.1(g) and 1(h), are

$$\begin{aligned}
M_{aK}^{V-A} = & -\frac{32\pi C_F M_B^4}{\sqrt{6}} \int_0^1 dx_1 dx_2 dx_3 \int_0^\infty b_1 db_1 b_2 db_2 \phi_{B_s}(x_1, b_1) \\
& \times \left\{ \left[ -x_2 \phi_\eta^A(x_2) \phi_K^A(x_3) - 4r_2 r_3 \phi_\eta^P(x_2) \phi_K^P(x_3) \right. \right. \\
& + r_2 r_3 (1 - x_2) (\phi_\eta^P(x_2) + \phi_\eta^T(x_2)) (\phi_K^P(x_3) - \phi_K^T(x_3)) \\
& + r_2 r_3 x_3 (\phi_\eta^P(x_2) - \phi_\eta^T(x_2)) (\phi_K^P(x_3) + \phi_K^T(x_3)) \left. \right] E'_a(t_d) h_{na}(x_1, x_2, x_3, b_1, b_2) \\
& + \left[ \bar{x}_3 \phi_\eta^A(x_2) \phi_K^A(x_3) + \bar{x}_3 r_2 r_3 (\phi_\eta^P(x_2) + \phi_\eta^T(x_2)) (\phi_K^P(x_3) - \phi_K^T(x_3)) \right. \\
& \left. \left. + x_2 r_2 r_3 (\phi_\eta^P(x_2) - \phi_\eta^T(x_2)) (\phi_K^P(x_3) + \phi_K^T(x_3)) \right] E'_a(t'_d) h'_{na}(x_1, x_2, x_3, b_1, b_2) \right\}, \quad (36)
\end{aligned}$$

$$\begin{aligned}
M_{aK}^{V+A} = & -\frac{32\pi C_F M_{B_s}^4}{\sqrt{6}} \int_0^1 dx_1 dx_2 dx_3 \int_0^\infty b_1 db_1 b_2 db_2 \phi_B(x_1, b_1) \\
& \times \left\{ \left[ r_2 (2 - x_2) (\phi_\eta^P(x_2) + \phi_\eta^T(x_2)) \phi_K^A(x_3) \right. \right. \\
& - r_3 (1 + x_3) \phi_\eta^A(x_2) (\phi_K^P(x_3) - \phi_K^T(x_3)) \left. \right] E'_a(t_d) h_{na}(x_1, x_2, x_3, b_1, b_2) \\
& + \left[ r_2 x_2 (\phi_\eta^P(x_2) + \phi_\eta^T(x_2)) \phi_K^A(x_3) - r_3 \bar{x}_3 \phi_\eta^A(x_2) (\phi_K^P(x_3) - \phi_K^T(x_3)) \right] \\
& \left. \times E'_a(t'_d) h'_{na}(x_1, x_2, x_3, b_1, b_2) \right\}, \quad (37)
\end{aligned}$$

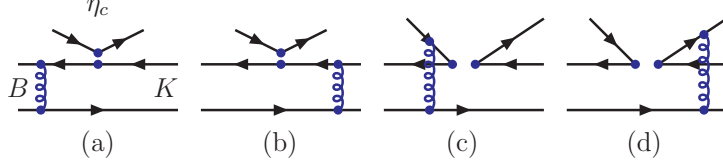


FIG. 2. Feynman diagrams which may contribute to the  $B \rightarrow K\eta_c$  decays in the pQCD approach at leading order.

$$\begin{aligned}
M_{aK}^{SP} = & -\frac{32\pi C_F M_B^4}{\sqrt{6}} \int_0^1 dx_1 dx_2 dx_3 \int_0^\infty b_1 db_1 b_2 db_2 \phi_B(x_1, b_1) \\
& \times \left\{ \left[ (x_3 - 1) \phi_\eta^A(x_2) \phi_K^A(x_3) - 4r_2 r_3 \phi_\eta^P(x_2) \phi_K^P(x_3) \right. \right. \\
& + r_2 r_3 x_3 (\phi_\eta^P(x_2) + \phi_\eta^T(x_2)) (\phi_K^P(x_3) - \phi_K^T(x_3)) \\
& + r_2 r_3 (1 - x_2) (\phi_\eta^P(x_2) - \phi_\eta^T(x_2)) (\phi_K^P(x_3) + \phi_K^T(x_3)) \left. \right] E'_a(t_d) h_{na}(x_1, x_2, x_3, b_1, b_2) \\
& + \left[ x_2 \phi_\eta^A(x_2) \phi_K^A(x_3) + x_2 r_2 r_3 (\phi_\eta^P(x_2) + \phi_\eta^T(x_2)) (\phi_K^P(x_3) - \phi_K^T(x_3)) \right. \\
& + r_2 r_3 (1 - x_3) (\phi_\eta^P(x_2) - \phi_\eta^T(x_2)) (\phi_K^P(x_3) + \phi_K^T(x_3)) \left. \right] \\
& \times E'_a(t'_d) h'_{na}(x_1, x_2, x_3, b_1, b_2) \left. \right\}, \tag{38}
\end{aligned}$$

The evolution functions  $E_i(t)$  and hard functions  $h_i$  appearing in Eqs. (29)-(38) are given explicitly in Appendix B.

If we exchange the position of  $K$  and  $\eta^{(\prime)}$  in Fig. 1, we will find the corresponding decay amplitudes for the case of  $B \rightarrow \eta^{(\prime)}$  transitions. Since the  $K$  and  $\eta^{(\prime)}$  are all pseudoscalar mesons and have the similar wave functions, the decay amplitudes for new diagrams – say  $F_{e\eta}^{V-A}$ ,  $F_{e\eta}^{V+A}$ ,  $F_{e\eta}^{SP}$ ,  $M_{e\eta}^{V-A}$ ,  $M_{e\eta}^{V+A}$ ,  $M_{e\eta}^{SP}$ ,  $F_{a\eta}^{V-A}$ ,  $F_{a\eta}^{V+A}$ ,  $F_{a\eta}^{SP}$ ,  $M_{a\eta}^{V-A}$ ,  $M_{a\eta}^{V+A}$ , and  $M_{a\eta}^{SP}$  – can be obtained from those as given in Eqs. (29)-(38) by the following replacements:

$$\phi_K^A \leftrightarrow \phi_{\eta^{(\prime)}}^A, \quad \phi_K^P \leftrightarrow \phi_{\eta^{(\prime)}}^P, \quad \phi_K^T \leftrightarrow \phi_{\eta^{(\prime)}}^T, \quad r_\eta \leftrightarrow r_K. \tag{39}$$

## B. $B \rightarrow K\eta_c$ at leading order

For  $B \rightarrow K\eta_c$  decays at leading order in the pQCD approach, the Feynman diagrams which may contribute are shown in Fig. 2. The  $B \rightarrow K\eta_c$  decays have been studied in Ref. [23] in the pQCD approach, at the full leading order and with the inclusion of the partial NLO vertex corrections. We here recalculated these decays and confirmed the

results of Ref. [23]. The relevant decay amplitudes are the following

$$\begin{aligned}
F_{\eta_c K} = & -8\pi C_F M_B^4 \int_0^1 dx_1 dx_3 \int_0^\infty db_1 db_3 \phi_B(x_1, b_1) \\
& \times \left\{ \left[ (1 - r_{\eta_c}^2)(1 + x_3) - x_3 r_{\eta_c}^2 \right] \phi_K^A(x_3) + r_3(1 - 2x_3) [\phi_K^P(x_3) + \phi_K^T(x_3)] \right. \\
& + r_3 r_{\eta_c}^2 [(1 + 2x_3) \phi_K^P(x_3) - (1 - 2x_3) \phi_K^T(x_3)] \left. E_e(t_e) h'_e(x_1, x_3, b_1, b_3) \right. \\
& \left. + 2r_3(1 - r_{\eta_c}^2) \phi_K^P(x_3) E_e(t'_e) h'_e(x_3, x_1, b_3, b_1) \right\}, \tag{40}
\end{aligned}$$

$$\begin{aligned}
M_{\eta_c K} = & \frac{32}{\sqrt{6}} \pi C_F M_B^4 \int_0^1 dx_1 dx_2 dx_3 \int_0^\infty db_1 db_2 \phi_B(x_1, b_1) \phi_{\eta_c}^\nu(x_2) \\
& \times \left[ x_3(1 - 2r_{\eta_c}^2) \phi_K^A(x_3) - 2x_3 r_3(1 - r_{\eta_c}^2) \phi_K^T(x_3) \right] \\
& \cdot E'_e(t'_f) h'_n(x_1, x_2, x_3, b_1, b_2), \tag{41}
\end{aligned}$$

where  $r_3 = m_0^K/m_B$ ,  $r_{\eta_c} = m_{\eta_c}/m_B$ , and  $r_c = m_c/m_B$ .  $\phi_{\eta_c}^\nu$  is the leading twist-2 part of the distribution amplitude for the pseudoscalar meson  $\eta_c$ . The evolution function  $E^{(\prime)}(t)$ , hard function  $h_i$  and the scale  $t_e$ ,  $t'_e$  are given in Appendix B.

In the leading-order pQCD approach, the total decay amplitude for the  $B \rightarrow \eta_c K$  decay can then be written as:

$$\begin{aligned}
\mathcal{M}(B \rightarrow \eta_c K) = & \frac{G_F}{\sqrt{2}} F_{\eta_c K} f_{\eta_c} \left[ V_{cb}^* V_{cs} a_2 - V_{tb}^* V_{ts} (a_3 - a_5 - a_7 + a_9) \right] \\
& + \frac{G_F}{\sqrt{2}} M_{\eta_c K} \left[ V_{cb}^* V_{cs} C_2 - V_{tb}^* V_{ts} (C_4 + C_6 + C_8 + C_{10}) \right], \tag{42}
\end{aligned}$$

where  $a_i$  is the combination of the Wilson coefficients  $C_i$ :

$$\begin{aligned}
a_{1,2} = & C_{2,1} + \frac{C_{1,2}}{3}; \quad a_i = C_i + \frac{C_{i+1}}{3}, \quad for \quad i = 3, 5, 7, 9; \\
a_i = & C_i + \frac{C_{i-1}}{3}, \quad for \quad i = 4, 6, 8, 10. \tag{43}
\end{aligned}$$

### C. Total decays amplitudes of $B \rightarrow K \eta^{(\prime)}$ decays

For  $B^0 \rightarrow K^0 \eta$  and  $B^+ \rightarrow K^+ \eta$  decays, by combining the contributions from all possible Feynman diagrams ( Figs. 1 and 2), one finds the general expressions for the total decay amplitudes (here the Wilson coefficients and Cabibbo-Kobayashi-Maskawa

(CKM) factors are all included),

$$\begin{aligned}
\mathcal{M}(K^0\eta) = & \frac{G_F}{\sqrt{2}} \left\{ \lambda_u \left[ a_2 f_\eta^q F_{eK}^{V-A} + C_2 M_{eK}^{V-A,q} F_1(\phi) \right] - \lambda_t \left( 2a_3 - 2a_5 - \frac{1}{2}a_7 + \frac{1}{2}a_9 \right) f_\eta^q F_{eK}^{V-A} \right. \\
& - \lambda_t \left[ \left( a_3 + a_4 - a_5 + \frac{1}{2}a_7 - \frac{1}{2}a_9 - \frac{1}{2}a_{10} \right) f_\eta^s F_{eK}^{V-A} \right. \\
& + \left( a_6 - \frac{1}{2}a_8 \right) [f_\eta^s F_{eK}^{SP} + f_B F_{aK}^{SP} F_2(\phi) + f_B F_{a\eta}^{SP} F_1(\phi) + f_K F_{e\eta}^{SP} F_1(\phi)] \\
& + \left( C_3 + C_4 - \frac{1}{2}C_9 - \frac{1}{2}C_{10} \right) M_{eK}^{V-A,s} F_2(\phi) \\
& + \left( 2C_4 + \frac{1}{2}C_{10} \right) M_{eK}^{V-A,q} F_1(\phi) + \left( C_5 - \frac{1}{2}C_7 \right) M_{eK}^{V+A,s} F_2(\phi) \\
& + \left( 2C_6 + \frac{1}{2}C_8 \right) M_{eK}^{SP,q} F_1(\phi) + \left( C_6 - \frac{1}{2}C_8 \right) M_{eK}^{SP,s} F_2(\phi) \\
& + \left( a_4 - \frac{1}{2}a_{10} \right) [f_B F_{aK}^{V-A} F_2(\phi) + f_K F_{e\eta}^{V-A} F_1(\phi) + f_B F_{a\eta}^{V-A} F_1(\phi)] \\
& + \left( C_3 - \frac{1}{2}C_9 \right) [M_{aK}^{V-A} F_2(\phi) + M_{e\eta}^{V-A} F_1(\phi) + M_{a\eta}^{V-A} F_1(\phi)] \\
& + \left. \left( C_5 - \frac{1}{2}C_7 \right) [M_{aK}^{V+A} F_2(\phi) + M_{e\eta}^{V+A} F_1(\phi) + M_{a\eta}^{V+A} F_1(\phi)] \right] \Big\} \\
& + \mathcal{M}(B \rightarrow \eta_c K) * F_c(\theta, \phi_G, \phi_Q), \tag{44}
\end{aligned}$$

$$\begin{aligned}
\mathcal{M}(K^+\eta) = & \frac{G_F}{\sqrt{2}} \left\{ \lambda_u \left[ a_2 f_\eta^q F_{eK}^{V-A} + C_2 M_{eK}^{V-A,q} F_1(\phi) + a_1 f_B [F_{aK}^{V-A} F_2(\phi) + F_{a\eta}^{V-A} F_1(\phi)] \right. \right. \\
& + a_1 f_K F_{e\eta}^{V-A} F_1(\phi) + C_1 [M_{aK}^{V-A} F_2(\phi) + M_{e\eta}^{V-A} F_1(\phi) + M_{a\eta}^{V-A} F_1(\phi)] \Big] \\
& - \lambda_t \left[ \left( 2a_3 - 2a_5 - \frac{1}{2}a_7 + \frac{1}{2}a_9 \right) f_\eta^q F_{eK}^{V-A} \right. \\
& + \left( a_3 + a_4 - a_5 + \frac{1}{2}a_7 - \frac{1}{2}a_9 - \frac{1}{2}a_{10} \right) f_\eta^s F_{eK}^{V-A} \\
& + \left( a_6 - \frac{1}{2}a_8 \right) f_\eta^s F_{eK}^{SP} + \left( C_3 + C_4 - \frac{1}{2}C_9 - \frac{1}{2}C_{10} \right) M_{eK}^{V-A,s} F_2(\phi) \\
& + \left( 2C_4 + \frac{1}{2}C_{10} \right) M_{eK}^{V-A,q} F_1(\phi) + \left( C_5 - \frac{1}{2}C_7 \right) M_{eK}^{V+A,s} F_2(\phi) \\
& + \left( 2C_6 + \frac{1}{2}C_8 \right) M_{eK}^{SP,q} F_1(\phi) + \left( C_6 - \frac{1}{2}C_8 \right) M_{eK}^{SP,s} F_2(\phi) \\
& + (a_4 + a_{10}) [f_B F_{aK}^{V-A} F_2(\phi) + f_K F_{e\eta}^{V-A} F_1(\phi) + f_B F_{a\eta}^{V-A} F_1(\phi)] \\
& + (a_6 + a_8) [f_B F_{aK}^{SP} F_2(\phi) + f_K F_{e\eta}^{SP} F_1(\phi) + f_B F_{a\eta}^{SP} F_1(\phi)] \\
& + (C_3 + C_9) [M_{aK}^{V-A} F_2(\phi) + M_{e\eta}^{V-A} F_1(\phi) + M_{a\eta}^{V-A} F_1(\phi)] \\
& + (C_5 + C_7) [M_{aK}^{V+A} F_2(\phi) + M_{e\eta}^{V+A} F_1(\phi) + M_{a\eta}^{V+A} F_1(\phi)] \Big] \Big\} \\
& + \mathcal{M}(B \rightarrow \eta_c K) * F_c(\theta, \phi_G, \phi_Q), \tag{45}
\end{aligned}$$

where  $\lambda_u = V_{ub}^* V_{us}$ ,  $\lambda_t = V_{tb}^* V_{ts}$ , and the Wilson coefficients  $a_i$  are the same as those defined in Eq. (43). The expressions for the mixing parameters  $F_i^{(\prime)}(\phi)$  depend on the choice of the different mixing schemes:

- (i) In MS-1, i.e., the FKS  $\eta$ - $\eta'$  mixing scheme, the mixing parameters  $F_{1,2}(\phi)$  and  $F'_{1,2}(\phi)$  are of the form

$$\sqrt{2}F_1(\phi) = F'_2(\phi) = \cos(\phi), \quad F_2(\phi) = -\sqrt{2}F'_1(\phi) = -\sin(\phi). \quad (46)$$

- (ii) In MS-2, i.e., the  $\eta$ - $\eta'$ - $G$  mixing scheme,  $F_{1,2}(\phi)$  and  $F'_{1,2}(\phi)$  are of the form

$$\begin{aligned} F_1(\phi) &= \frac{1}{\sqrt{2}}(\cos \phi + \sin \theta \sin \theta_i \Delta_G), & F_2(\phi) &= -\sin \phi + \sin \theta \cos \theta_i \Delta_G, \\ F'_1(\phi) &= \frac{1}{\sqrt{2}}(\sin \phi - \cos \theta \sin \theta_i \Delta_G), & F'_2(\phi) &= \cos \phi - \cos \theta \cos \theta_i \Delta_G. \end{aligned} \quad (47)$$

- (iii) In MS-3, i.e., the third  $\eta$ - $\eta'$ - $G$ - $\eta_c$  mixing scheme,  $F_{1,2}(\phi)$  and  $F'_{1,2}(\phi)$  are the same as those defined in Eq. (47). For this case, the  $\eta_c$  also contribute through mixing, and the relevant mixing parameters are

$$F_c(\theta, \phi_G, \phi_Q) = -\sin \theta \sin \phi_G \sin \phi_Q, \quad F'_c(\theta, \phi_G, \phi_Q) = \cos \theta \sin \phi_G \sin \phi_Q. \quad (48)$$

Finally, the total decay amplitudes for  $B^0 \rightarrow K^0 \eta'$  and  $B^+ \rightarrow K^+ \eta'$  in the pQCD approach at leading order can be obtained easily from Eqs. (44) and (45) by the following replacements:

$$f_\eta^q \rightarrow f_{\eta'}^q, \quad f_\eta^s \rightarrow f_{\eta'}^s, \quad F_1(\phi) \rightarrow F'_1(\phi), \quad F_2(\phi) \rightarrow F'_2(\phi), \quad F_c(\phi) \rightarrow F'_c(\phi). \quad (49)$$

## IV. NLO CONTRIBUTIONS IN THE PQCD APPROACH

In this section we will present the total decay amplitudes for  $B \rightarrow K \eta^{(\prime)}$  decays in the pQCD approach with the inclusion of all currently known NLO contributions.

### A. General analysis of the NLO contributions in the pQCD approach

As is well known, the power-counting rule in the pQCD factorization approach [21] is rather different from that in the QCD factorization [7, 36, 37]. When compared with the previous LO calculations in pQCD [9], the full pQCD predictions should include the following NLO contributions:

- (1) We should use the Wilson coefficients  $C_i(m_W)$  at the NLO level in the naive dimensional regularization scheme [29], the NLO renormalization group (RG) evolution matrix  $U(t, m, \alpha)$  as defined in Ref. [29], and the strong-coupling constant  $\alpha_s(t)$  at the two-loop level.

- (2) Besides the LO hard kernel  $H^{(0)}(\alpha_s)$ , all the Feynman diagrams, that contribute to  $H^{(1)}(\alpha_s^2)$  in the pQCD approach, should be considered. The typical Feynman diagrams which contribute to  $H^{(1)}(\alpha_s^2)$  at the NLO level in the pQCD approach are shown in Figs. 3-5, and can be classified into six types.
- (i) The vertex correction: the NLO contributions from the Feynman diagrams as shown in Figs.3(a)-3(d), which were evaluated ten years ago[21, 36, 37].
  - (ii) The quark loops: the NLO contributions from the quark loops as shown in Figs. 3(e)-3(f), the relevant analytical formulas can be found in Ref. [21].
  - (iii) The magnetic penguins: the NLO contributions from the operator  $O_{8g}$ , as shown in Figs.3(g)-3(h). These Feynman diagrams were evaluated several years ago [38].
  - (iv) The NLO form factors(FF): i.e., the NLO contributions to the  $B \rightarrow P$  transition form factors  $F_0^{B \rightarrow P}(0)$  with  $P = (K, \eta_q)$  in this paper. The typical relevant Feynman diagrams are shown in Fig. 4, and were calculated very recently in Ref. [14].
  - (v) The NLO contributions from the spectator diagrams as shown in Figs. 5(a)-5(d), which are obtained by adding a new gluon line between any two quark lines in Figs. 1(c) and 1(d), or by replacing the one-gluon lines with a three-gluon vertex in Figs. 1(c) and 1(d). Such contributions are still unknown now.
  - (vi) The NLO contributions from the annihilation diagrams, as shown by Figs. 5(e)-5(h), which are obtained by adding a new gluon line between any two quark lines in Figs. 1(e)-1(h). Such contributions are also unknown now.

The NLO contributions from the Feynman diagrams in Fig. 3 – the vertex corrections, the quark-loops and chromo-magnetic penguins – were evaluated several years ago [21, 36, 38], and taken into account in our previous studies for the  $B \rightarrow K\eta^{(\prime)}$  decay in Ref. [12].

The Feynman diagrams as shown in Fig. 4 can provide the NLO contributions to the  $B \rightarrow P$  transition form factors and have been calculated very recently in Ref. [14]. The authors of Ref.[14] calculated the NLO corrections to the  $B \rightarrow \pi$  transition form factors in the leading twist in the  $k_T$  factorization theorem, and they found that the NLO part can provide a 20 – 30% enhancement to the LO results for the corresponding form factors. Since  $\pi, K$  and  $\eta^{(\prime)}$  are all pseudoscalar mesons and have similar wave functions, it is straightforward to extend the calculations in Ref. [14] to the cases for the  $B \rightarrow K, \eta^{(\prime)}$  transition form factors. In this paper, we will consider the effects of the NLO part of the form factors. According to general expectations, the enhanced form factors may lead to a larger branching ratio for  $B \rightarrow K\eta^{(\prime)}$  decays.

The still-missing NLO parts in the pQCD approach are the  $O(\alpha_s^2)$  contributions from nonfactorizable spectator diagrams and annihilation diagrams, as illustrated by Figs. 5(a)-5(h). The analytical calculations for these Feynman diagrams are still absent at present. But it is generally believed that the NLO contributions from these Feynman diagrams should be small

- (i) The contributions from the nonfactorizable spectator diagrams in Figs. 1(c) and 1(d), their contributions at leading order are strongly suppressed by the isospin symmetry and color suppression with respect to the factorizable emission diagrams



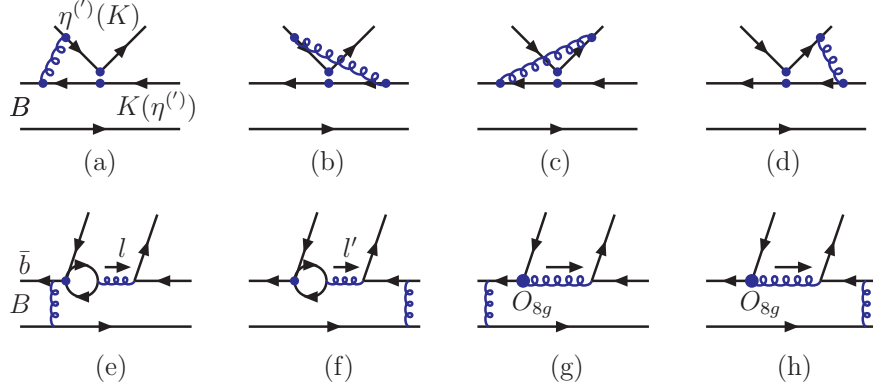


FIG. 3. The typical Feynman diagrams that provide NLO contributions to  $B \rightarrow K\eta^{(\prime)}$  decays in the pQCD approach: (a)-(d) are the vertex corrections, (e)-(f) are the quark-loops, and (g)-(h) are the chromo-magnetic Penguins  $O_{sg}$ .

Figs. 1(a) and 1(b). The NLO contributions from Figs. 5(a)-5(d) are higher-order effects on small LO quantities, and therefore should be much smaller than the LO ones.

- (ii) The annihilation spectator diagrams at leading order, i.e., Figs. 1(e)-1(h), they are power suppressed and generally much smaller with respect to the contributions from the emission diagrams Figs.1(a) and 1(b). The contributions from Figs. 5(a)-5(d) are also the higher-order corrections to the small quantities and therefore should be much smaller than its LO parts.

In the next section, we will explicitly evaluate the numerical values of the individual decay amplitudes corresponding to different Feynman diagrams, and will compare the size of every part of the total decay amplitude for the considered decays. We will try to make a simple and clear comparison between the contributions from different sets of Feynman diagrams or from the different sources numerically.

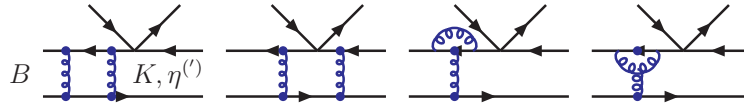


FIG. 4. The typical Feynman diagrams that may provide NLO contributions to  $B \rightarrow P$  form factors.

## B. The NLO contributions to $B \rightarrow K\eta^{(\prime)}$ decays

In Ref. [12], by using the ordinary FKS  $\eta - \eta^{(\prime)}$  mixing scheme, we calculated the branching ratios and CP-violating asymmetries of the four  $B \rightarrow K\eta^{(\prime)}$  decays at leading order and partial next-to-leading order, i.e., the NLO contributions from the Feynman diagrams in Fig. 3 were taken into account in Ref. [12]. For details about the calculations of these NLO contributions and the expressions of their relevant functions, we refer the reader to Ref. [12]. For the sake of the reader, we here give a brief summary of these “old” NLO parts.

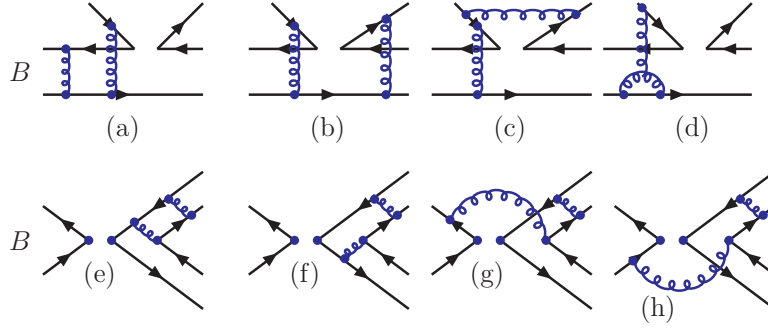


FIG. 5. The typical Feynman diagrams that may provide NLO contributions to  $B \rightarrow K\eta^{(\prime)}$  decays in the pQCD approach: (a)-(d) are the spectator diagrams, (e)-(h) are the annihilation diagrams.

(a) **Vertex corrections(VC):**

The vertex corrections to the factorizable emission diagrams, as illustrated by Figs. 2(a)-2(d), were calculated years ago in the QCD factorization approach[7, 36, 37]. The difference between the cases that do or do not consider the parton transverse momentum  $k_T$  are very small and can be neglected[21]. The NLO vertex corrections will be included by adding a vertex function  $V_i(M)$  to the corresponding Wilson coefficients  $a_i(\mu)$  [36, 37],

$$\begin{aligned} a_{1,2}(\mu) &\rightarrow a_{1,2}(\mu) + \frac{\alpha_s(\mu)}{4\pi} C_F \frac{C_{1,2}(\mu)}{3} V_{1,2}(M), \\ a_i(\mu) &\rightarrow a_i(\mu) + \frac{\alpha_s(\mu)}{4\pi} C_F \frac{C_{i+1}(\mu)}{3} V_i(M), \quad \text{for } i = 3, 5, 7, 9, \\ a_i(\mu) &\rightarrow a_i(\mu) + \frac{\alpha_s(\mu)}{4\pi} C_F \frac{C_{i-1}(\mu)}{3} V_i(M), \quad \text{for } i = 4, 6, 8, 10, \end{aligned} \quad (50)$$

where  $M$  is the meson emitted from the weak vertex. When  $M$  is a pseudoscalar meson, the vertex functions  $V_i(M)$  can be written as [21, 37]:

$$V_i(M) = \begin{cases} 12 \ln \frac{m_b}{\mu} - 18 + \frac{2\sqrt{6}}{f_M} \int_0^1 dx \phi_M^A(x) g(x), & \text{for } i = 1 - 4, 9, 10, \\ -12 \ln \frac{m_b}{\mu} + 6 - \frac{2\sqrt{6}}{f_M} \int_0^1 dx \phi_M^A(x) g(1-x), & \text{for } i = 5, 7, \\ -6 + \frac{2\sqrt{6}}{f_M} \int_0^1 dx \phi_M^P(x) h(x), & \text{for } i = 6, 8, \end{cases} \quad (51)$$

where  $f_M$  is the decay constant of the meson  $M$ , and the hard-scattering functions  $g(x)$  and  $h(x)$  can be found in Ref. [12].

(b) **Quark loops(QL):**

The contribution from the so-called “quark loops” is a kind of penguin correction with the insertion of the four quark operators, as illustrated by Figs. 3(e) and 3(f). We here include the quark-loop amplitudes from the operators  $O_{1,2}$  and  $O_{3-6}$  only. The quark loops from  $O_{7-10}$  will be neglected due to their smallness.

For the  $\bar{b} \rightarrow \bar{s}$  transition, the contributions from the various quark loops are given by:

$$H_{eff}^{(ql)} = - \sum_{q=u,c,t} \sum_{q'} \frac{G_F}{\sqrt{2}} V_{qb}^* V_{qs} \frac{\alpha_s(\mu)}{2\pi} C^q(\mu, l^2) (\bar{b} \gamma_\rho (1 - \gamma_5) T^a s) (\bar{q}' \gamma^\rho T^a q'), \quad (52)$$

where  $l^2$  is the invariant mass of the gluon, which attaches the quark loops in Figs. 3(e) and 3(f). The functions  $C^q(\mu, l^2)$  can be found in Ref. [12]. The “quark-loop” contribution to the considered  $B \rightarrow K \eta^{(\prime)}$  decays can be written as [12]

$$M_{K\eta}^{(ql)} = \langle K\eta | \mathcal{H}_{eff}^{ql} | B \rangle = \frac{G_F}{\sqrt{2}} \sum_{q=u,c,t} V_{qb}^* V_{qs} \left[ M_{K\eta_s}^{(q)} F_2(\phi) + M_{\eta_q K}^{(q)} F_1(\phi) \right], \quad (53)$$

$$M_{K\eta'}^{(ql)} = \langle K\eta' | \mathcal{H}_{eff}^{(ql)} | B \rangle = \frac{G_F}{\sqrt{2}} \sum_{q=u,c,t} V_{qb}^* V_{qs} \left[ M_{K\eta_s}^{(q)} F'_2(\phi) + M_{\eta_q K}^{(q)} F'_1(\phi) \right], \quad (54)$$

where  $F_{1,2}^{(\prime)}(\phi)$  are the mixing parameters ( which have been defined in previous sections), while the decay amplitudes  $M_{K\eta_s}^{(q)}$  and  $M_{\eta_q K}^{(q)}$  are of the form [12]

$$\begin{aligned} M_{K\eta_s}^{(q)} = & \frac{8}{\sqrt{6}} C_F^2 m_B^4 \int_0^1 dx_1 dx_2 dx_3 \int_0^\infty b_1 db_1 b_3 db_3 \phi_B(x_1, b_1) \\ & \cdot \left\{ \left[ (1+x_3) \phi_K^A(x_3) \phi_{\eta_s}^A(x_2) + r_K (1-2x_3) (\phi_K^P(x_3) + \phi_K^T(x_3)) \phi_{\eta_s}^A(x_2) \right. \right. \\ & + 2r_{\eta_s} \phi_K^A(x_3) \phi_{\eta_s}^P(x_2) + 2r_K r_{\eta_s} ((2+x_3) \phi_K^P(x_3) - x_3 \phi_K^T(x_3)) \phi_{\eta_s}^P(x_2) \Big] \\ & \cdot E^{(q)}(t_q, l^2) h_e(x_1, x_3, b_1, b_3) \\ & + \left[ 2r_K \phi_K^P(x_3) \phi_{\eta_s}^A(x_2) + 4r_K r_{\eta_s} \phi_K^P(x_3) \phi_{\eta_s}^P(x_2) \right] \\ & \cdot E^{(q)}(t'_q, l'^2) h_e(x_3, x_1, b_3, b_1) \Big\}, \end{aligned} \quad (55)$$

for the  $B \rightarrow K$  transition, and

$$\begin{aligned} M_{\eta_q K}^{(q)} = & \frac{8}{\sqrt{6}} C_F^2 m_B^4 \int_0^1 dx_1 dx_2 dx_3 \int_0^\infty b_1 db_1 b_3 db_3 \phi_B(x_1, b_1) \\ & \cdot \left\{ \left[ (1+x_3) \phi_{\eta_q}^A(x_3) \phi_K^A(x_2) + r_\eta (1-2x_3) (\phi_{\eta_q}^P(x_3) + \phi_{\eta_q}^T(x_3)) \phi_K^A(x_2) \right. \right. \\ & + 2r_K \phi_{\eta_q}^A(x_3) \phi_K^P(x_2) + 2r_\eta r_K ((2+x_3) \phi_{\eta_q}^P(x_3) - x_3 \phi_{\eta_q}^T(x_3)) \phi_K^P(x_2) \Big] \\ & \cdot E^{(q)}(t_q, l^2) h_e(x_1, x_3, b_1, b_3) \\ & + \left[ 2r_\eta \phi_{\eta_q}^P(x_3) \phi_K^A(x_2) + 4r_\eta r_K \phi_{\eta_q}^P(x_3) \phi_K^P(x_2) \right] \\ & \cdot E^{(q)}(t'_q, l'^2) h_e(x_3, x_1, b_3, b_1) \Big\}, \end{aligned} \quad (56)$$

for the  $B \rightarrow \eta$  transition. Here  $r_\eta = m_0^q/m_B$  and  $r_{\eta_s} = m_0^s/m_B$ . The expressions for the evolution functions  $E^{(q)}(t_q, l^2)$  and  $E^{(q)}(t'_q, l'^2)$ , as well as the hard functions  $h_e(x_1, x_3, b_1, b_3)$  and  $h_e(x_3, x_1, b_3, b_1)$  can be found in Ref. [12].

(c) **Chromo-magnetic penguins(MP):**

This is another kind of penguin correction but with the insertion of  $O_{8g}$ . The corresponding effective weak Hamiltonian for the  $\bar{b} \rightarrow \bar{s}g$  transition is of the form[21],

$$H_{eff}^{cmp} = -\frac{G_F}{\sqrt{2}} \frac{g_s}{8\pi^2} m_b V_{tb}^* V_{ts} C_{8g}^{eff} \bar{b}_i \sigma^{\mu\nu} (1 - \gamma_5) T_{ij}^a G_{\mu\nu}^a s_j, \quad (57)$$

where the effective Wilson coefficient  $C_{8g}^{eff} = C_{8g} + C_5$  [21]. The total chromo-magnetic penguin contribution to the considered  $B \rightarrow K\eta^{(\prime)}$  decays can be written as

$$M_{K\eta}^{(cmp)} = \langle K\eta | \mathcal{H}_{eff}^{cmp} | B \rangle = -\frac{G_F}{\sqrt{2}} \lambda_t \left[ M_{K\eta_s}^{(g)} F_2(\phi) + M_{\eta_q K}^{(g)} F_1(\phi) \right], \quad (58)$$

$$M_{K\eta'}^{(cmp)} = \langle K\eta' | \mathcal{H}_{eff}^{cmp} | B \rangle = -\frac{G_F}{\sqrt{2}} \lambda_t \left[ M_{K\eta_s}^{(g)} F_2'(\phi) + M_{\eta_q K}^{(g)} F_1'(\phi) \right], \quad (59)$$

where the mixing parameters  $F_{1,2}^{(\prime)}(\phi)$  have been defined in Sec.II. The decay amplitudes  $M_{K\eta_s}^{(g)}$  and  $M_{\eta_q K}^{(g)}$  are obtained by evaluating the Feynman diagrams Figs. 3(g) and 3(h)[12],

$$\begin{aligned} M_{K\eta_s}^{(g)} = & -\frac{8}{\sqrt{6}} C_F^2 m_B^6 \int_0^1 dx_1 dx_2 dx_3 \int_0^\infty b_1 db_1 b_2 db_2 b_3 db_3 \phi_B(x_1, b_1) \\ & \cdot \left\{ \left\{ 2(-1+x_3)\phi_{\eta_s}^A(x_2)\phi_K^A(x_3) + r_{\eta_s}x_2(1+x_3)[-3\phi_{\eta_s}^P(x_2) + \phi_{\eta_s}^T(x_2)]\phi_K^A(x_3) \right. \right. \\ & + r_K[(-3+2x_3+x_3^2)\phi_K^P(x_3) + (-1+2x_3-x_3^2)\phi_K^T(x_3)]\phi_{\eta_s}^A(x_2) \\ & + 3r_{\eta_s}r_K[(-1-x_2+x_3+2x_2x_3)\phi_K^P(x_3) + (1-x_2-x_3+2x_2x_3)\phi_K^T(x_3)]\phi_{\eta_s}^P(x_2) \\ & \left. + r_{\eta_s}r_K[(-1+x_2+x_3-2x_2x_3)\phi_K^P(x_3) + (1+x_2-x_3-2x_2x_3)\phi_K^T(x_3)]\phi_{\eta_s}^T(x_2) \right\} \\ & \cdot E_g(t_q)h_g(A, B, C, b_1, b_3, b_2, x_3) \\ & - [4r_K\phi_{\eta_s}^A(x_2)\phi_K^P(x_3) + 2r_{\eta_s}r_Kx_2\phi_K^P(x_3)(3\phi_{\eta_s}^P(x_2) - \phi_{\eta_s}^T(x_2))] \\ & \cdot E_g(t'_q)h_g(A', B', C', b_3, b_1, b_2, x_1) \Big\}, \end{aligned} \quad (60)$$

$$\begin{aligned} M_{K\eta_q}^{(g)} = & -\frac{8}{\sqrt{6}} C_F^2 m_B^6 \int_0^1 dx_1 dx_2 dx_3 \int_0^\infty b_1 db_1 b_2 db_2 b_3 db_3 \phi_B(x_1, b_1) \\ & \cdot \left\{ \left\{ 2(-1+x_3)\phi_K^A(x_2)\phi_{\eta_q}^A(x_3) + r_Kx_2(1+x_3)[-3\phi_K^P(x_2) + \phi_K^T(x_2)]\phi_{\eta_q}^A(x_3) \right. \right. \\ & + r_{\eta_q}[(-3+2x_3+x_3^2)\phi_{\eta_q}^P(x_3) + (-1+2x_3-x_3^2)\phi_{\eta_q}^T(x_3)]\phi_K^A(x_2) \\ & + 3r_{\eta_q}r_K[(-1-x_2+x_3+2x_2x_3)\phi_{\eta_q}^P(x_3) + (1-x_2-x_3+2x_2x_3)\phi_{\eta_q}^T(x_3)]\phi_K^P(x_2) \\ & \left. + r_{\eta_q}r_K[(-1+x_2+x_3-2x_2x_3)\phi_{\eta_q}^P(x_3) + (1+x_2-x_3-2x_2x_3)\phi_{\eta_q}^T(x_3)]\phi_K^T(x_2) \right\} \\ & \cdot E_g(t_q)h_g(A, B, C, b_1, b_3, b_2, x_3) \\ & - [4r_{\eta_q}\phi_K^A(x_2)\phi_{\eta_q}^P(x_3) + 2r_{\eta_q}r_Kx_2\phi_{\eta_q}^P(x_3)(3\phi_K^P(x_2) - \phi_K^T(x_2))] \\ & \cdot E_g(t'_q)h_g(A', B', C', b_3, b_1, b_2, x_1) \Big\}, \end{aligned} \quad (61)$$

where  $r_\eta = m_0^q/m_B$ ,  $r_{\eta_s} = m_0^s/m_B$ , and  $r_K = m_0^K/m_B$ . The explicit expressions of the evolution functions  $E_g$  and the hard functions  $h_g$  in Eqs. (60) and (61) can be easily found in Ref. [12].

### C. The form factors at NLO level

As mentioned in the Introduction, Li et al. derived the  $k_T$ -dependent NLO hard kernel  $H^{(1)}$  for the  $B \rightarrow \pi$  transition form factor [14]. We here extend their results for the  $B \rightarrow \pi$  form factors to the ones for  $B \rightarrow K$  and  $B \rightarrow (\eta_q, \eta_s)$  transitions, under the assumption of  $SU(3)$  flavor symmetry. As given in Eq.(56) of Ref. [14], the NLO hard kernel  $H^{(1)}$  can be written as

$$\begin{aligned} H^{(1)} &= F(x_1, x_3, \mu, \mu_f, \eta, \zeta_1) H^{(0)} \\ &= \frac{\alpha_s(\mu_f) C_F}{4\pi} \left[ \frac{21}{4} \ln \frac{\mu^2}{m_B^2} - \left( \ln \frac{m_B^2}{\zeta_1^2} + \frac{13}{2} \right) \ln \frac{\mu_f^2}{m_B^2} + \frac{7}{16} \ln^2(x_1 x_3) + \frac{1}{8} \ln^2 x_1 \right. \\ &\quad + \frac{1}{4} \ln x_1 \ln x_3 + \left( 2 \ln \frac{m_B^2}{\zeta_1^2} + \frac{7}{8} \ln \eta - \frac{1}{4} \right) \ln x_1 + \left( \frac{7}{8} \ln \eta - \frac{3}{2} \right) \ln x_3 \\ &\quad \left. + \left( \frac{15}{4} - \frac{7}{16} \ln \eta \right) \ln \eta - \frac{1}{2} \ln \frac{m_B^2}{\zeta_1^2} \left( 3 \ln \frac{m_B^2}{\zeta_1^2} + 2 \right) + \frac{101}{48} \pi^2 + \frac{219}{16} \right] H^{(0)}, \quad (62) \end{aligned}$$

where the scale  $\zeta_1 = 25m_B$ , and  $\eta = 1 - (p_1 - p_3)^2/m_B^2$  is the energy fraction carried by the meson that picks up the spectator quark. For  $B \rightarrow K\eta_q, K\eta_s$  decays, the large recoil region corresponds to the energy fraction  $\eta \sim O(1)$ . For  $B \rightarrow K\eta_c$ ,  $\eta(K) \sim (1 - r_{\eta_c}^2)$ .  $\mu_f$  is the factorization scale, which is set to be the hard scales

$$t^a = \max(\sqrt{x_3 \eta} m_B, 1/b_1, 1/b_3), \quad \text{or} \quad t^b = \max(\sqrt{x_1 \eta} m_B, 1/b_1, 1/b_3), \quad (63)$$

corresponding to the largest energy scales in Figs. 1(a) and 1(b), respectively. The renormalization scale  $\mu$  is defined as [14]

$$\mu = t_s(\mu_f) = \left\{ \text{Exp} \left[ c_1 + \left( \ln \frac{m_B^2}{\zeta_1^2} + \frac{5}{4} \right) \ln \frac{\mu_f^2}{m_B^2} \right] x_1^{c_2} x_3^{c_3} \right\}^{2/21} \mu_f, \quad (64)$$

with the coefficients

$$\begin{aligned} c_1 &= - \left( \frac{15}{4} - \frac{7}{16} \ln \eta \right) \ln \eta + \frac{1}{2} \ln \frac{m_B^2}{\zeta_1^2} \left( 3 \ln \frac{m_B^2}{\zeta_1^2} + 2 \right) - \frac{101}{48} \pi^2 - \frac{219}{16}, \\ c_2 &= - \left( 2 \ln \frac{m_B^2}{\zeta_1^2} + \frac{7}{8} \ln \eta - \frac{1}{4} \right), \\ c_3 &= - \frac{7}{8} \ln \eta + \frac{3}{2}. \end{aligned}$$

At the NLO level, the hard kernel function  $H$  can then be written as

$$H = H^{(0)}(\alpha_s) + H^{(1)}(\alpha_s^2) = [1 + F(x_1, x_3, \mu, \mu_f, \eta, \zeta_1)] H^{(0)}(\alpha_s). \quad (65)$$

## D. The NLO contributions to $B \rightarrow K\eta_c$ decays

For  $B \rightarrow \eta_c K$  decays, the NLO contributions include two parts: (a) the NLO vertex corrections to these decays, which have been taken into account in Ref. [23]; and (b) the NLO contributions to the  $B \rightarrow K$  transition form factors, which is the newly known NLO part.

Since the emitted meson is  $\eta_c = c\bar{c}$ , the soft and collinear infrared divergences of the four-vertex correction diagrams will cancel each other. So these vertex corrections can be calculated without considering the transverse-momentum effects of the quark at the end-point region, the same way as in the collinear factorization theorem.

The NLO vertex corrections can be included through the redefinition of the Wilson coefficients:

$$\begin{aligned} a_2 &\rightarrow a_2 + \frac{\alpha_s}{4\pi} C_F \frac{C_2}{3} (-18 + 12 \ln \frac{m_b}{\mu} + f_I), \\ a_i &\rightarrow a_i + \frac{\alpha_s}{4\pi} C_F \frac{C_{i+1}}{3} (-18 + 12 \ln \frac{m_b}{\mu} + f_I), \quad \text{for } i = 3, 9, \\ a_j &\rightarrow a_j - \frac{\alpha_s}{4\pi} C_F \frac{C_{j+1}(\mu)}{3} (-6 + 12 \ln \frac{m_b}{\mu} + f_I), \quad \text{for } j = 5, 7, \end{aligned} \quad (66)$$

where the function  $f_I$  is of the form

$$f_I = \frac{2\sqrt{2N_c}}{f_{\eta_c}} \int_0^1 dx \phi_{\eta_c}^\nu(x) \left[ \frac{3(1-2x)}{1-x} \ln x + 3(\ln(1-z) - i\pi) + \frac{2z(1-x)}{1-zx} \right], \quad (67)$$

where  $z = m_{\eta_c}^2/m_B^2$ .

The NLO contributions to the  $B \rightarrow K$  transition form factors can be included for the  $B \rightarrow K\eta_c$  decay in the same way as for  $B \rightarrow K\eta^{(\prime)}$  decays.

## V. NUMERICAL RESULTS AND DISCUSSIONS

### A. Input parameters

We use the following input parameters [10, 11] in the numerical calculations (all masses and decay constants are in units of GeV):

$$\begin{aligned} f_B &= 0.21, \quad f_K = 0.16, \quad f_{\eta_c} = 0.4874, \quad m_\eta = 0.5475, \quad m_{\eta'} = 0.9578, \\ m_{K^0} &= 0.498, \quad m_{K^+} = 0.494, \quad m_{0K} = 1.7, \quad M_B = 5.28, \\ m_b &= 4.8, \quad m_c = 1.5, \quad m_{\eta_c} = 2.98, \\ M_W &= 80.41, \quad \tau_{B^0} = 1.53\text{ps}, \quad \tau_{B^+} = 1.638\text{ps}. \end{aligned} \quad (68)$$

For the CKM quark-mixing matrix, we adopt the Wolfenstein parametrization as given in Ref. [10, 11],

$$\begin{aligned} V_{ud} &= 0.9748, \quad V_{us} = \lambda = 0.2246, \quad |V_{ub}| = 3.61 \times 10^{-3}, \\ V_{cd} &= -0.225, \quad V_{cs} = 0.9748, \quad V_{cb} = 0.04197, \\ |V_{td}| &= 8.8 \times 10^{-3}, \quad V_{ts} = -0.042, \quad V_{tb} \approx 1.0, \end{aligned} \quad (69)$$

with the CKM parameters:  $\lambda = 0.2246 \pm 0.0011$ ,  $A = 0.832 \pm 0.017$ ,  $\bar{\rho} = 0.130 \pm 0.018$ , and  $\bar{\eta} = 0.350 \pm 0.013$ .

## B. Form factors at LO and NLO level

We first calculate and present the pQCD predictions for the form factors at zero momentum transfer for  $B \rightarrow K\eta^{(\prime)}$  decays at the LO and NLO levels, respectively. In the calculation, we consider three different mixing schemes respectively.

In this paper the form factors  $F_0^{B \rightarrow \eta}(0)$  and  $F_0^{B \rightarrow \eta'}(0)$  are defined as

$$\begin{aligned} F_0^{B \rightarrow \eta}(0) &= \cos \phi F_0^{B \rightarrow \eta_q}(0)_I, \\ F_0^{B \rightarrow \eta'}(0) &= \sin(\phi) F_0^{B \rightarrow \eta_q}(0)_I, \end{aligned} \quad (70)$$

in the ordinary FKS  $\eta - \eta'$  mixing scheme, and

$$\begin{aligned} F_0^{B \rightarrow \eta}(0) &= [\cos \phi + \sin \theta \sin \theta_i (1 - \cos \phi_G)] F_0^{B \rightarrow \eta_q}(0)_{II}, \\ F_0^{B \rightarrow \eta'}(0) &= [\sin \phi - \cos \theta \sin \theta_i (1 - \cos \phi_G)] F_0^{B \rightarrow \eta_q}(0)_{II}, \end{aligned} \quad (71)$$

in the MS-2 and MS-3 mixing schemes. One should note that the form factor  $F_0^{B \rightarrow \eta_q}(0)_I$  is different from  $F_0^{B \rightarrow \eta_q}(0)_{II}$  since some relevant parameters in the distribution amplitudes, such as  $\rho_{\eta_q} = 2m_q/m_{qq}$ , are different in different mixing schemes. The pQCD predictions for the numerical values of the form factors for three different mixing schemes are all listed in Table I, and they are obtained by using the central values of all input parameters. For the relevant mixing angles, we take  $\phi = 39.3^\circ$  in the MS-1 mixing scheme; while we take  $\theta_i = 54.7^\circ$ ,  $\theta = -11^\circ$ ,  $\phi = \theta + \theta_i = 43.7^\circ$  and  $\phi_G = 12^\circ$  in both the MS-2 and MS-3 mixing schemes. The error comes from the uncertainty of  $\omega_b = 0.40 \pm 0.04$  GeV.

TABLE I. The LO and NLO pQCD predictions for the form factors of the  $B \rightarrow K\eta^{(\prime)}$  decays for three different mixing schemes.

Form factors	MS	LO	NLO
$F_0^{B \rightarrow \eta_q}(0)$	1	0.20	$0.26 \pm 0.04$
	2,3	0.28	$0.33 \pm 0.06$
$F_0^{B \rightarrow K}(0)$	all	0.37	$0.43^{+0.07}_{-0.05}$

From the numerical values of the form factors in Table. I, we can see that (a) the form factors are the same for the  $\eta$ - $\eta'$ - $G$  mixing scheme and the  $\eta$ - $\eta'$ - $G$ - $\eta_c$  mixing scheme, since the  $\eta_c$  component in the  $\eta$ - $\eta'$ - $G$ - $\eta_c$  mixing scheme does not affect the evaluation of the form factors  $F_0^{B \rightarrow \eta^{(\prime)}}(0)$  and  $F_0^{B \rightarrow K}(0)$ ; and (b) the NLO contributions also provide  $\sim 20\%$  enhancements to the corresponding form factors.

## C. $Br(B \rightarrow K\eta^{(\prime)})$ in the $\eta$ - $\eta'$ mixing scheme

In the B rest frame, the branching ratio of a general  $B \rightarrow M_2 M_3$  decay can be written as

$$Br(B \rightarrow M_2 M_3) = \tau_B \frac{1}{16\pi m_B} \chi |\mathcal{M}(B \rightarrow M_2 M_3)|^2, \quad (72)$$

where  $\tau_B$  is the lifetime of B meson and  $\chi \approx 1$  is the phase space factor, which is equal to unit when the masses of final-state light mesons are neglected.

Using the input parameters and the wave functions as given in previous sections, it is straightforward to calculate the CP-averaged branching ratios for the four  $B \rightarrow K\eta^{(\prime)}$  decays considered in different mixing schemes. For the case of the ordinary  $\eta - \eta'$  mixing scheme, the pQCD predictions are listed in Table. II, where the label “NLO-1” refers to the pQCD predictions with the inclusion of the same set of NLO contributions as in Ref. [12]. The label “NLO” in Table II means that all currently known NLO contributions are included, especially the NLO part of the form factor obtained by evaluating the Feynman diagrams as shown in Fig. 4 [14]. For comparison, we also list the corresponding experimental measurements [10] and the theoretical predictions in the pQCD approach [12] and in the QCD factorization (QCDF) approach [37].

TABLE II. The pQCD predictions for the branching ratios (in units of  $10^{-6}$ ) in the ordinary  $\eta - \eta'$  mixing scheme with  $\phi = 39.3^\circ$ . The label “NLO” means that all currently known NLO contributions are included.

Channel	LO	NLO-1	NLO	Data[10]	pQCD[12]	QCDF[37]
$B^0 \rightarrow K^0 \eta$	2.12	2.76	$2.62^{+3.6}_{-1.7}$	$1.23^{+0.27}_{-0.24}$	$2.1^{+2.6}_{-1.5}$	$1.1^{+2.4}_{-1.5}$
$B^0 \rightarrow K^0 \eta'$	27.9	48.3	$57.2^{+23.7}_{-17.0}$	$66.1 \pm 3.1$	$50.3^{+16.8}_{-10.6}$	$46.5^{+41.9}_{-22.0}$
$B^+ \rightarrow K^+ \eta$	3.83	3.78	$4.0^{+3.8}_{-2.2}$	$2.4^{+0.22}_{-0.21}$	$3.2^{+3.2}_{-1.8}$	$1.9^{+3.0}_{-1.9}$
$B^+ \rightarrow K^+ \eta'$	30.3	49.8	$58.7^{+24.0}_{-17.2}$	$71.1 \pm 2.6$	$51.0^{+18.0}_{-10.9}$	$49.1^{+45.2}_{-23.6}$

Of course, the NLO pQCD predictions for the CP-averaged branching ratios still have large theoretical uncertainties. If we take into account the effects of the uncertainties of the main input parameters, we find that

$$\begin{aligned}
Br(B^0 \rightarrow K^0 \eta) &= [2.62^{+1.22}_{-0.78}(\omega_b)^{+2.49}_{-1.04}(m_s)^{+0.52}_{-0.48}(f_B)^{+1.37}_{-1.04}(a_2^\eta)] \times 10^{-6}, \\
Br(B^0 \rightarrow K^0 \eta') &= [57.2^{+16.1}_{-11.2}(\omega_b)^{+12.6}_{-7.00}(m_s)^{+11.4}_{-10.4}(f_B)^{+3.49}_{-2.42}(a_2^\eta)] \times 10^{-6}, \\
Br(B^+ \rightarrow K^+ \eta) &= [3.97^{+1.67}_{-1.13}(\omega_b)^{+2.97}_{-1.30}(m_s)^{+0.79}_{-0.72}(f_B)^{+1.57}_{-1.20}(a_2^\eta)] \times 10^{-6}, \\
Br(B^+ \rightarrow K^+ \eta') &= [58.7^{+16.2}_{-11.2}(\omega_b)^{+13.0}_{-7.20}(m_s)^{+11.7}_{-10.6}(f_B)^{+3.17}_{-2.18}(a_2^\eta)] \times 10^{-6}, \quad (73)
\end{aligned}$$

where the major errors are induced by the uncertainties of  $\omega_b = 0.4 \pm 0.04$  GeV,  $m_s = 0.13 \pm 0.03$  GeV,  $f_B = 0.21 \pm 0.02$  GeV, and the Gegenbauer moment  $a_2^\eta = 0.44 \pm 0.22$  (here  $a_2^\eta$  denotes  $a_2^{\eta_q}$  or  $a_2^{\eta_s}$ ), respectively. The total theoretical errors in the NLO pQCD predictions as shown in the fourth column of Table II are obtained by adding the four individual theoretical errors in quadrature. From the numerical results as given in Eq. (73) and Table II we make the following points.

- (i) By comparing the predictions as listed in the “NLO-1” column and the “NLO” column, one can see that the inclusion of the NLO contributions in the form factors can provide an 18% enhancement to  $Br(B \rightarrow K\eta')$ . The gap between the pQCD predictions and the measured values therefore becomes effectively marrow, but there is still a small difference between the central values of the pQCD predictions and the data.



- (ii) For  $B \rightarrow K\eta$  decays, however, the pQCD predictions for their branching ratios remain basically unchanged after the inclusion of the NLO part of the form factors. Although the NLO pQCD predictions for  $Br(B \rightarrow K\eta)$  are consistent with the data within one standard deviation, the central values of the NLO pQCD predictions are still larger than the measured values by almost a factor of 2.
- (iii) The pQCD predictions as given in the NLO-1 column agree well with those presented in Ref. [12] (i.e. the results as listed in the “pQCD” column of Table II), and the small differences are induced by the variations of some input parameters, such as the CKM matrix elements.
- (iv) Although the NLO pQCD predictions for  $Br(B \rightarrow K\eta)$  and  $Br(B \rightarrow K\eta')$  are consistent with the data within one standard deviation, here we cannot provide a good interpretation for the observed pattern of  $Br(B \rightarrow k\eta^{(\prime)})$  in the FKS  $\eta$ - $\eta'$  mixing scheme.

#### D. $Br(B \rightarrow K\eta^{(\prime)})$ in the $\eta$ - $\eta'$ - $G$ mixing scheme

In the  $\eta$ - $\eta'$ - $G$  mixing scheme, by using the input parameters and the wave functions as given in previous sections and fixing the mixing parameters  $\theta = -11^\circ$ ,  $\phi = 43.7^\circ$  and  $\phi_G = 12^\circ$ , we find the LO and NLO pQCD predictions for the CP-averaged branching ratios as listed in Table III. As a comparison, we also show the measured values and the QCDF predictions as given in Ref. [37] in the last two columns of the Table III.

TABLE III. The same as in Table I but for the case of the  $\eta$ - $\eta'$ - $G$  mixing scheme with the mixing parameters  $\phi = 43.7^\circ$ ,  $\theta = -11^\circ$ ,  $\theta_i = 54.7^\circ$ , and  $\phi_G = 12^\circ$ .

Channel	LO	NLO-1	NLO	Data[10]	QCDF[37]
$B^0 \rightarrow K^0\eta$	0.90	1.15	$1.13^{+2.0}_{-1.0}$	$1.23^{+0.27}_{-0.24}$	$1.1^{+2.4}_{-1.5}$
$B^0 \rightarrow K^0\eta'$	35.2	57.4	$66.5^{+25.9}_{-15.4}$	$66.1 \pm 3.1$	$46.5^{+41.9}_{-22.0}$
$B^+ \rightarrow K^+\eta$	1.98	2.10	$2.36^{+2.6}_{-1.5}$	$2.36^{+0.22}_{-0.21}$	$1.9^{+3.0}_{-1.9}$
$B^+ \rightarrow K^+\eta'$	38.9	58.3	$67.3^{+26.0}_{-19.4}$	$71.1 \pm 2.6$	$49.1^{+45.2}_{-23.6}$

The NLO pQCD predictions with the inclusion of the major theoretical errors are the following:

$$\begin{aligned}
Br(B^0 \rightarrow K^0\eta) &= [1.13^{+0.50}_{-0.32}(\omega_b)^{+1.60}_{-0.67}(m_s)^{+0.23}_{-0.20}(f_B)^{+0.99}_{-0.69}(a_2^\eta)] \times 10^{-6}, \\
Br(B^0 \rightarrow K^0\eta') &= [66.5^{+19.6}_{-13.6}(\omega_b)^{+9.9}_{-6.4}(m_s)^{+13.3}_{-12.1}(f_B)^{+3.0}_{-2.1}(a_2^\eta)] \times 10^{-6}, \\
Br(B^+ \rightarrow K^+\eta) &= [2.36^{+0.97}_{-0.61}(\omega_b)^{+2.05}_{-0.94}(m_s)^{+0.47}_{-0.43}(f_B)^{+1.25}_{-0.90}(a_2^\eta)] \times 10^{-6}, \\
Br(B^+ \rightarrow K^+\eta') &= [67.3^{+19.6}_{-13.5}(\omega_b)^{+10.2}_{-6.4}(m_s)^{+13.4}_{-12.2}(f_B)^{+2.7}_{-1.8}(a_2^\eta)] \times 10^{-6}. \quad (74)
\end{aligned}$$

Analogous to the case of MS-1, the major theoretical errors in the MS-2 mixing scheme are still induced by the uncertainties of the input parameters:  $\omega_b = 0.4 \pm 0.04$  GeV,  $m_s = 0.11 \pm 0.02$  GeV,  $f_B = 0.21 \pm 0.02$  GeV, and Gegenbauer moment  $a_2^\eta = 0.44 \pm 0.22$ . The total theoretical errors of the NLO pQCD predictions in the fourth column of Table

III are obtained by adding the four individual theoretical errors in quadrature. One can make the following points from the numerical results in Eq. (74) and Table III that

- (i) In the  $\eta$ - $\eta'$ - $G$  mixing scheme, the glueball part plays an important role in improving the agreement between the pQCD predictions and the data. Even at the leading order, the pQCD predictions for  $Br(B \rightarrow K\eta')$  ( $Br(B \rightarrow K\eta)$ ) become larger (smaller) than those in the case of MS-1. The corresponding changes are what we need to interpret the data.
- (ii) For the  $B^0 \rightarrow K^0\eta'$  ( $B^+ \rightarrow K^+\eta'$ ) decay, the NLO contribution provides a 89% (73%) enhancement to its branching ratio with respect to the LO prediction. The NLO part of the form factors along provide a 23% enhancement to the corresponding branching ratios. The NLO pQCD predictions for both  $Br(B^0 \rightarrow K^0\eta')$  and  $Br(B^+ \rightarrow K^+\eta')$  are now in full agreement with the data.
- (iii) For both  $B^0 \rightarrow K^0\eta$  and  $B^+ \rightarrow K^+\eta$  decays, the NLO enhancements are small in size, and the agreement between the pQCD predictions and the data also improved effectively due to the inclusion of all of the known NLO contributions.
- (iv) For all four  $B \rightarrow K\eta^{(\prime)}$  decays considered, the differences between the numerical values as listed in the NLO-1 column and the NLO column in Table III show the effects of the inclusion of the NLO part of the form factors. It is easy to see that the NLO pQCD predictions for the branching ratios are in perfect agreement with the measured values due to the contribution from the glueball component in the  $\eta$ - $\eta'$ - $G$  mixing scheme and the inclusion of the NLO contributions.

#### E. $Br(B \rightarrow K\eta^{(\prime)})$ in the “ $\eta$ - $\eta'$ - $G$ - $\eta_c$ ” mixing scheme

In the “ $\eta$ - $\eta'$ - $G$ - $\eta_c$ ” mixing scheme, by using the input parameters and the wave functions as given in previous sections and fixing the mixing parameters  $\theta = -11^\circ$ ,  $\phi = 43.7^\circ$ ,  $\phi_G = 12^\circ$  and  $\phi_Q = 11^\circ$ , we find the LO and NLO pQCD predictions for the CP-averaged branching ratios, which are listed in Table IV.

TABLE IV. The same as in Table I but for the case of the “ $\eta$ - $\eta'$ - $G$ - $\eta_c$ ” mixing scheme. The label NLO means that all known NLO contributions are included.

Channel	LO	NLO-1	NLO	Data[10]	QCDF[37]
$B^0 \rightarrow K^0\eta$	0.67	0.87	$0.82^{+1.8}_{-0.8}$	$1.23^{+0.27}_{-0.24}$	$1.1^{+2.4}_{-1.5}$
$B^0 \rightarrow K^0\eta'$	43.5	55.6	$64.8^{+26.8}_{-20.4}$	$66.1 \pm 3.1$	$46.5^{+41.9}_{-22.0}$
$B^+ \rightarrow K^+\eta$	1.50	2.00	$2.19^{+2.5}_{-1.4}$	$2.36^{+0.22}_{-0.21}$	$1.9^{+3.0}_{-1.9}$
$B^+ \rightarrow K^+\eta'$	51.7	56.2	$65.2^{+27.0}_{-20.0}$	$71.1 \pm 2.6$	$49.1^{+45.2}_{-23.6}$

In the “ $\eta$ - $\eta'$ - $G$ - $\eta_c$ ” mixing scheme, the contributions from the decay chain  $B \rightarrow K\eta_c \rightarrow K\eta^{(\prime)}$  are included. The NLO pQCD predictions for the CP-averaged branching ratios

with the major theoretical errors are of the form

$$\begin{aligned}
Br(B^0 \rightarrow K^0 \eta) &= [0.82_{-0.18}^{+0.29}(\omega_b)_{-0.57}^{+1.47}(m_s)_{-0.14}^{+0.17}(f_B)_{-0.55}^{+0.92}(a_2^\eta)] \times 10^{-6}, \\
Br(B^0 \rightarrow K^0 \eta') &= [64.8_{-14.7}^{+21.2}(\omega_b)_{-6.5}^{+10.3}(m_s)_{-11.8}^{+12.9}(f_B)] \times 10^{-6}, \\
Br(B^+ \rightarrow K^+ \eta) &= [2.19_{-0.54}^{+0.75}(\omega_b)_{-0.95}^{+2.06}(m_s)_{-0.40}^{+0.44}(f_B)_{-0.86}^{+1.19}(a_2^\eta)] \times 10^{-6}, \\
Br(B^+ \rightarrow K^+ \eta') &= [65.2_{-14.7}^{+21.2}(\omega_b)_{-6.8}^{+10.6}(m_s)_{-11.8}^{+13.0}(f_B)] \times 10^{-6}.
\end{aligned} \tag{75}$$

Analogous to the cases of the  $\eta$ - $\eta'$  and  $\eta$ - $\eta'$ - $G$  mixing schemes, the major errors here are also induced by the uncertainties of  $\omega_b$ ,  $m_s$ ,  $f_B$ , and the Gegenbauer coefficient  $a_2^\eta$ , respectively. For  $B \rightarrow K\eta'$  decays, however, the error induced by the uncertainty of  $a_2^\eta = 0.44 \pm 0.22$  is very small and has been neglected. The total theoretical errors of the NLO pQCD predictions in the fourth column of Table IV are obtained by adding the individual theoretical errors in quadrature.

From Table IV, one can see that the NLO pQCD predictions for  $Br(B \rightarrow K\eta')$  also agree well with the data. For  $B \rightarrow K\eta$  decays, although the central values of the NLO pQCD predictions for  $Br(B \rightarrow K\eta)$  are a little smaller than the measured values, but they are still consistent with the data within one standard deviation. Since the values of the relevant mixing parameters  $F_C(\theta, \phi_G, \phi_Q)$  and  $F'_C(\theta, \phi_G, \phi_Q)$  as defined in Eq. (49) are all very small,

$$F_C(\theta, \phi_G, \phi_Q) = 0.0076, \quad F'_C(\theta, \phi_G, \phi_Q) = 0.039, \tag{76}$$

for  $(\theta, \phi_G, \phi_Q) = (-11^\circ, 12^\circ, 11^\circ)$ , the  $\eta_c$  contributions to the  $B \rightarrow K\eta^{(\prime)}$  decays are indeed very small.

## F. CP-violating asymmetries

Now we turn to the evaluations of the CP-violating asymmetries of  $B \rightarrow K\eta^{(\prime)}$  decays in the pQCD approach. For  $B^+ \rightarrow K^+\eta^{(\prime)}$  decays, the direct CP-violating asymmetries  $\mathcal{A}_{CP}^{\text{dir}}$  can be defined as:

$$\mathcal{A}_{CP}^{\text{dir}} = \frac{\Gamma(\bar{B}^0 \rightarrow \bar{f}) - \Gamma(B^0 \rightarrow f)}{\Gamma(\bar{B}^0 \rightarrow \bar{f}) + \Gamma(B^0 \rightarrow f)} = \frac{|\overline{\mathcal{M}}_f|^2 - |\mathcal{M}_f|^2}{|\overline{\mathcal{M}}_f|^2 + |\mathcal{M}_f|^2}, \tag{77}$$

Using the input parameters and the wave functions as given in previous sections, it is easy to calculate the direct CP-violating asymmetries for the considered decays, which are listed in Table V. The major theoretical errors as given in Table V are induced by the uncertainties of the input parameters of  $\omega_b$ ,  $m_s$ , and  $a_2^\eta$ . As a comparison, we also list currently available data [10] and the corresponding QCDF predictions [37]. The label “NLO” means that all known NLO contributions are taken into account. For  $B^\pm \rightarrow K^\pm \eta$  decays, there is a large direct CP asymmetry ( $\mathcal{A}_{CP}^{\text{dir}}$ ), due to the destructive interference between the penguin amplitude and the tree amplitude.

From the pQCD predictions and the relevant data as listed in Table V, one can see the following.

- (i) For  $B^\pm \rightarrow K^\pm \eta$  decays, the LO pQCD predictions for  $\mathcal{A}_{CP}^{\text{dir}}$  in all three mixing schemes have a sign opposite that of the measured value. The inclusion of the NLO

TABLE V. The LO and NLO pQCD predictions for the direct CP asymmetries  $\mathcal{A}_{CP}^{\text{dir}}(B^\pm \rightarrow K^\pm \eta)$  and  $\mathcal{A}_{CP}^{\text{dir}}(B^\pm \rightarrow K^\pm \eta')$  in the three different mixing schemes (in units of  $10^{-2}$ ).

Mode	MS	LO	NLO	Data[10]	QCDF[37]
$\mathcal{A}_{CP}^{\text{dir}}(K^\pm \eta)$	1	10.0	$-25.2_{-1.8}^{+2.7}(\omega_b)_{-12.3}^{+10.9}(m_s)_{-12.2}^{+8.0}(a_2^\eta)$	$-37 \pm 8$	$-18.9_{-30.0}^{+29.0}$
	2	31.1	$-22.9_{-5.2}^{+7.6}(\omega_b)_{-16.7}^{+11.6}(m_s)_{-7.6}^{+6.3}(a_2^\eta)$		
	3	42.4	$-2.8_{-8.5}^{+8.5}(\omega_b)_{-3.3}^{+1.9}(m_s)_{-3.3}^{+8.4}(a_2^\eta)$		
$\mathcal{A}_{CP}^{\text{dir}}(K^\pm \eta')$	1	-10.4	$-4.4_{-0.6}^{+0.7}(\omega_b)_{-0.8}^{+1.1}(m_s)_{-1.3}^{+1.5}(a_2^\eta)$	$1.3_{-1.7}^{+1.6}$	$-9.0_{-16.2}^{+10.6}$
	2	-12.2	$-5.5_{-0.8}^{+0.8}(\omega_b)_{-0.7}^{+0.9}(m_s)_{-1.5}^{+1.5}(a_2^\eta)$		
	3	-9.0	$-2.3_{-1.1}^{+1.1}(\omega_b)_{-0.4}^{+0.4}(m_s)_{-1.6}^{+1.4}(a_2^\eta)$		

contributions changes the sign of the pQCD prediction for  $\mathcal{A}_{CP}^{\text{dir}}$ , and the NLO pQCD predictions for  $\mathcal{A}_{CP}^{\text{dir}}(B^\pm \rightarrow K^\pm \eta)$  in the cases of MS-1 and MS-2 become consistent with the data within one standard deviation. In the “ $\eta$ - $\eta'$ - $G$ ” mixing scheme, for example, the NLO pQCD predictions are of the form

$$\begin{aligned}\mathcal{A}_{CP}^{\text{dir}}(B^\pm \rightarrow K^\pm \eta) &= (-22.9_{-19.1}^{+15.2}) \times 10^{-2}, \\ \mathcal{A}_{CP}^{\text{mix}}(B^\pm \rightarrow K^\pm \eta') &= (-5.5_{-1.8}^{+1.9}) \times 10^{-2},\end{aligned}\tag{78}$$

where the individual errors as shown in Table V are added in quadrature.

- (ii) In the case of MS-3, however, the pQCD prediction for  $\mathcal{A}_{CP}^{\text{dir}}(B^\pm \rightarrow K^\pm \eta)$  changes its sign after the inclusion of the NLO contributions. The NLO pQCD prediction is of the form

$$\mathcal{A}_{CP}^{\text{dir}}(B^\pm \rightarrow K^\pm \eta') = (-2.8_{-9.7}^{+10.7}) \times 10^{-2},\tag{79}$$

which is still much smaller in magnitude than the measured value in magnitude. There is a clear difference between the pQCD prediction and the data for  $\mathcal{A}_{CP}^{\text{dir}}(B^\pm \rightarrow K^\pm \eta')$  in the “ $\eta$ - $\eta'$ - $G$ - $\eta_c$ ” mixing scheme.

- (iii) For  $B^\pm \rightarrow K^\pm \eta'$  decays, the measured value of  $\mathcal{A}_{CP}^{\text{dir}}(K^\pm \eta') = 1.3_{-1.7}^{+1.6} \times 10^{-2}$  is consistent with zero. The NLO pQCD predictions in the three different mixing schemes agree well with the data within one standard deviation, while the consistency between the pQCD predictions and the data are effectively improved by the inclusion of the NLO contributions.

As for the CP-violating asymmetries for the neutral decays  $B^0 \rightarrow K^0 \eta^{(\prime)}$ , the effects of  $B^0 - \bar{B}^0$  mixing should be considered. The CP-violating asymmetry of  $B^0(\bar{B}^0) \rightarrow K^0 \eta^{(\prime)}$  decays are time dependent and can be defined as

$$A_{CP} \equiv \frac{\Gamma_{\bar{B}_d^0 \rightarrow f}(\Delta t) - \Gamma_{B_d^0 \rightarrow f}(\Delta t)}{\Gamma_{\bar{B}_d^0 \rightarrow f}(\Delta t) + \Gamma_{B_d^0 \rightarrow f}(\Delta t)} = \mathcal{C}_f \cos(\Delta m \Delta t) + \mathcal{S}_f \sin(\Delta m \Delta t),\tag{80}$$

where  $\Delta m$  is the mass difference between the two  $B_d^0$  mass eigenstates, and  $\Delta t = t_{CP} - t_{tag}$  is the time difference between the tagged  $B^0$  ( $\overline{B}^0$ ) and the accompanying  $\overline{B}^0$  ( $B^0$ ) with opposite b flavor decaying to the final CP-eigenstate  $f_{CP}$  at the time  $t_{CP}$ . The direct and mixing-induced CP-violating asymmetries  $\mathcal{C}_f$  ( or  $\mathcal{A}_f$  as used by the Belle Collaboration) and  $\mathcal{S}_f$  can be written as

$$\mathcal{A}_{CP}^{dir} = \mathcal{C}_f \equiv \frac{|\lambda|^2 - 1}{1 + |\lambda|^2}, \quad \mathcal{A}_{CP}^{mix} = \mathcal{S}_f \equiv \frac{2\text{Im}(\lambda)}{1 + |\lambda|^2}, \quad (81)$$

with the CP-violating parameter  $\lambda$

$$\lambda \equiv \left(\frac{q}{p}\right)_d \cdot \frac{\langle f | H_{eff} | \overline{B}^0 \rangle}{\langle f | H_{eff} | B^0 \rangle}. \quad (82)$$

By integrating the time variable  $t$ , one finds the total CP asymmetries for  $B^0 \rightarrow K^0 \eta^{(\prime)}$  decays,

$$\mathcal{A}_{CP}^{tot} = \frac{1}{1 + x^2} \mathcal{A}_{CP}^{dir} + \frac{x}{1 + x^2} \mathcal{A}_{CP}^{mix}, \quad (83)$$

where  $x = \Delta m / \Gamma = 0.774$  [11].

In Table VI, we show the LO and NLO pQCD predictions for the direct, the mixing-induced, and the total CP asymmetries for  $B^0 \rightarrow K_S^0 \eta^{(\prime)}$  decays in the three different mixing schemes. Analogous to the NLO pQCD predictions for the branching ratios, the label “NLO” here means that the inclusion of all currently known NLO contributions are taken into account.

From the pQCD predictions and currently available experimental measurements for the CP-violating asymmetries of  $B^0 \rightarrow K_S^0 \eta^{(\prime)}$  decays, one can see the following.

- (i) Unlike the cases for the branching ratios, the pQCD predictions for the CP-violating asymmetries of the neutral  $B^0 \rightarrow K_S^0 \eta^{(\prime)}$  decays are not sensitive to both the NLO contributions and the choice of the mixing schemes.
- (ii) The NLO pQCD predictions for  $\mathcal{A}_{CP}^{dir}(B^0 \rightarrow K_S^0 \eta')$  and  $\mathcal{A}_{CP}^{mix}(B^0 \rightarrow K_S^0 \eta')$  have small theoretical error and agree very well with the measured values:

$$\begin{aligned} \mathcal{A}_{CP}^{dir}(B^0 \rightarrow K_S^0 \eta') &= (3.3 \pm 0.3(\text{theory})) \times 10^{-2}, \\ \mathcal{A}_{CP}^{mix}(B^0 \rightarrow K_S^0 \eta') &= (70.3 \pm 0.5(\text{theory})) \times 10^{-2}, \end{aligned} \quad (84)$$

while the measured values are  $(1 \pm 9)\%$  and  $(64 \pm 11)\%$ , respectively.

- (iii) The pQCD predictions of  $\mathcal{A}_{CP}^{dir}(B^0 \rightarrow K_S^0 \eta) \sim -16\%$  and  $\mathcal{A}_{CP}^{mix}(B^0 \rightarrow K_S^0 \eta) \sim 67\%$  will be tested by the LHCb and the forthcoming Super-B experiments.

TABLE VI. The pQCD predictions for the direct-, mixing-induced and total CP asymmetries (in units of  $10^{-2}$ ) for  $B^0 \rightarrow K^0 \eta^{(\prime)}$  decays in three different mixing schemes, and the world averages as given by HFAG [10].

Mode	MS	LO	NLO	Data
$\mathcal{A}_{CP}^{dir}(B^0 \rightarrow K_S^0 \eta)$	1	-4.6	$-11.1_{-0.7}^{+0.7}(\omega_b)_{-2.0}^{+2.9}(m_s)_{-3.3}^{+2.6}(a_2^\eta)$	—
	2	-6.6	$-16.0_{-0.8}^{+0.9}(\omega_b)_{-7.8}^{+5.8}(m_s)_{-11.9}^{+5.3}(a_2^\eta)$	—
	3	-7.8	$-19.4_{-0.0}^{+0.8}(\omega_b)_{-16.2}^{+8.1}(m_s)_{-16.7}^{+7.4}(a_2^\eta)$	—
$\mathcal{A}_{CP}^{mix}(B^0 \rightarrow K_S^0 \eta)$	1	69.3	$66.3_{-0.3}^{+0.5}(\omega_b)_{-3.3}^{+2.4}(m_s)_{-3.9}^{+2.2}(a_2^\eta)$	—
	2	69.9	$66.7_{-1.5}^{+1.5}(\omega_b)_{-6.5}^{+2.6}(m_s)_{-5.2}^{+2.2}(a_2^\eta)$	—
	3	70.3	$69.5_{-2.0}^{+2.1}(\omega_b)_{-2.8}^{+0.8}(m_s)_{-0.5}^{+2.6}(a_2^\eta)$	—
$\mathcal{A}_{CP}^{tot}(B^0 \rightarrow K_S^0 \eta)$	1	30.6	$25.2_{-0.2}^{+0.3}(\omega_b)_{-2.9}^{+3.0}(m_s)_{-4.0}^{+2.7}(a_2^\eta)$	—
	2	29.7	$22.3_{-0.0}^{+0.2}(\omega_b)_{-8.1}^{+4.8}(m_s)_{-9.9}^{+4.4}(a_2^\eta)$	—
	3	29.2	$21.6_{-1.0}^{+1.5}(\omega_b)_{-11.5}^{+5.5}(m_s)_{-9.2}^{+4.9}(a_2^\eta)$	—
$\mathcal{A}_{CP}^{dir}(B^0 \rightarrow K_S^0 \eta')$	1	1.1	$3.4_{-0.2}^{+0.2}(\omega_b)_{-0.2}^{+0.1}(m_s)_{-0.1}^{+0.1}(a_2^\eta)$	—
	2	1.0	$3.3_{-0.2}^{+0.1}(\omega_b)_{-0.1}^{+0.1}(m_s)_{-0.1}^{+0.1}(a_2^\eta)$	$1 \pm 9$
	3	0.9	$3.5_{-0.1}^{+0.1}(\omega_b)_{-0.2}^{+0.1}(m_s)_{-0.2}^{+0.2}(a_2^\eta)$	—
$\mathcal{A}_{CP}^{mix}(B^0 \rightarrow K_S^0 \eta')$	1	70.7	$69.8_{-0.1}^{+0.1}(\omega_b)_{-0.1}^{+0.2}(m_s)_{-0.2}^{+0.2}(a_2^\eta)$	—
	2	70.8	$70.0_{-0.1}^{+0.1}(\omega_b)_{-0.1}^{+0.1}(m_s)_{-0.1}^{+0.1}(a_2^\eta)$	$64 \pm 11$
	3	70.8	$70.5_{-0.1}^{+0.1}(\omega_b)_{-0.0}^{+0.1}(m_s)_{-0.1}^{+0.1}(a_2^\eta)$	—
$\mathcal{A}_{CP}^{tot}(B^0 \rightarrow K_S^0 \eta')$	1	34.9	$35.9_{-0.2}^{+0.2}(\omega_b)_{-0.0}^{+0.0}(m_s)_{-0.0}^{+0.0}(a_2^\eta)$	—
	2	34.9	$36.0_{-0.2}^{+0.1}(\omega_b)_{-0.0}^{+0.0}(m_s)_{-0.0}^{+0.0}(a_2^\eta)$	—
	3	34.8	$36.3_{-0.1}^{+0.1}(\omega_b)_{-0.1}^{+0.1}(m_s)_{-0.1}^{+0.1}(a_2^\eta)$	—

### G. Relative strength of the contributions from different sources

In the pQCD approach at leading order, we usually have the following general expectations:

- (a) The factorizable emission diagrams Figs. 1(a) and 1(b) provide the dominant contribution to the considered  $B \rightarrow K \eta^{(\prime)}$  decays;
- (b) The nonfactorizable spectator diagrams Figs. 1(c) and 1(d) are strongly suppressed by both the isospin cancelation and the color suppression and therefore play a minor role;
- (c) The annihilation diagrams Figs. 1(e)-1(h) are generally power suppressed in magnitude, but may provide a large strong phase to produce large CP-violating asymmetries for some decay modes.

In the pQCD approach at next-to-leading order, as discussed in previous sections, we have made two assumptions.

- (a) The currently known NLO contributions to  $H^{(1)}(\alpha_s^2)$  — such as those coming from

the Feynman diagrams as shown in Figs. 3 and 4 – are the dominant part of the full NLO contribution.

- (b) The still missing parts of the NLO contributions from the spectator and annihilation diagrams as shown in Fig. 5 are small in size and can be safely neglected.

Of course, these two assumptions should be examined properly before the analytic calculations for the missing parts are performed. For this purpose, we take the four  $B \rightarrow K\eta^{(\prime)}$  decays as an example, and try to check about the relative strength of the LO or currently known NLO contributions coming from different sources.

If the LO contributions ( $\propto \mathcal{O}(\alpha_s)$ ) from the nonfactorizable spectator diagrams Figs. 1(c) and 1(d) and the annihilation diagrams Figs. 1(e)-1(h) are already much smaller in size when compared with those from the factorizable emission diagrams Figs. 1(a)-1(b), it is reasonable for us to assume that the still missing next-to-leading order  $\mathcal{O}(\alpha_s^2)$  corrections coming from Figs. 5(a)-5(h) should be smaller than their counterparts at leading order, and therefore much smaller than those dominant LO contributions; they can therefore be neglected safely.

In order to check whether these general expectations or assumptions are correct, we here will firstly decompose the LO decay amplitude  $\mathcal{M}_{LO}$  into different parts according to the corresponding Feynman diagrams, and then make numerical evaluations for each part and compare their magnitudes directly. We try to make a simple and clear numerical comparison between the contributions from different sources.

For the  $B^+ \rightarrow K^+\eta$  decay in the  $\eta$ - $\eta'$  mixing scheme, for example, the decay amplitude  $\mathcal{M}(B^+ \rightarrow K^+\eta)$  at leading order as given in Eq. (45)<sup>2</sup> can be rewritten as a sum of three parts

$$\mathcal{M}_{LO}(B^+ \rightarrow K^+\eta) = \mathcal{M}^{a+b}(K^+\eta) + \mathcal{M}^{c+d}(K^+\eta) + \mathcal{M}^{anni}(K^+\eta), \quad (85)$$

where the decay amplitude  $\mathcal{M}^{a+b}$  is obtained by evaluating the dominant emission diagrams Figs. 1(a) and 1(b),  $\mathcal{M}^{c+d}$  refers to the LO contribution from the spectator diagrams Figs. 1(c) and 1(d), while  $\mathcal{M}^{anni}$  denotes the LO contribution from the annihilation diagrams Figs. 1(e)-1(h).

By using the central values of the input parameters and the relevant wave functions, we make the numerical calculations step by step and then find the numerical results (in units of  $10^{-4}$ )

$$\begin{aligned} \mathcal{M}_{LO}(B^+ \rightarrow K^+\eta) &= \underbrace{-1.76 - i0.37}_{\mathcal{M}^{a+b}} + \underbrace{0.065 - i0.14}_{\mathcal{M}^{c+d}} + \underbrace{0.03 + i0.57}_{\mathcal{M}^{anni}} \\ &= -1.67 + i0.062. \end{aligned} \quad (86)$$

It is easy to see the following.

- (a)  $\mathcal{M}^{a+b} = (-1.76 - i0.37) \times 10^{-4}$  is indeed large and dominant;
- (b)  $\mathcal{M}^{c+d} = (0.065 - i0.14) \times 10^{-4}$ : its real and imaginary parts are all much smaller than the corresponding parts of both  $\mathcal{M}^{a+b}$  and  $\mathcal{M}^{anni}$ ;

---

<sup>2</sup> In the  $\eta$ - $\eta'$  and  $\eta$ - $\eta'$ - $G$  mixing schemes, the last term  $\mathcal{M}(B \rightarrow \eta_c K) \cdot F_c(\theta, \phi_G, \phi_Q)$  in Eq. (45) is absent.

- (c)  $\mathcal{M}^{\text{anni}} = (0.03 + i0.57) \times 10^{-4}$ ; its real part is close to zero, but its imaginary part is large and interferes destructively with  $\mathcal{M}^{a+b}$ .

Since the branching ratio of the considered decays are proportional to the square of the decays amplitude  $|\mathcal{M}|^2$ , as shown by Eq. (72), we can define the relative strength of the individual contribution from different sources as the ratio  $R_{LO}$  and then compare the numerical results directly:

$$\begin{aligned} R_{LO}(K^+\eta) &= |\mathcal{M}^{a+b}|^2 : |\mathcal{M}^{c+d}|^2 : |\mathcal{M}^{\text{anni}}|^2 : |\mathcal{M}_{LO}|^2 \\ &= 3.23 : 0.02 : 0.33 : 2.79. \end{aligned} \quad (87)$$

One can see directly from the above numbers that the contribution from  $\mathcal{M}^{c+d}$  is less than 1% and can be safely neglected, while the contributions from  $\mathcal{M}^{\text{anni}}$  is also small in magnitude – around 10% of the dominant contribution from emission diagram [ Figs. 1(a) and 1(b)]. This hierarchy of the contributions from different sources agrees very well with the general expectations, as stated in the beginning of this subsection.

Using the same methods, we make the similar decompositions and numerical calculations for the remaining three decay modes  $B^0 \rightarrow K^0\eta^{(\prime)}$  and  $B^+ \rightarrow K^+\eta^{(\prime)}$ , and find the numerical values of the decay amplitudes and the relative strength. We make the calculations in both the  $\eta$ - $\eta'$  and  $\eta$ - $\eta'$ - $G$  mixing schemes and show all the numerical results in Table VII. For the case of each mixing scheme we use the same input parameters as those used in the calculation for the branching ratios in Secs.V C and V D , respectively.

TABLE VII. The LO pQCD predictions for the numerical values (in unit of  $10^{-4}$ ) of the individual and total decay amplitudes of  $B^0 \rightarrow K^0\eta^{(\prime)}$  and  $B^+ \rightarrow K^+\eta^{(\prime)}$  decays, and in the  $\eta$ - $\eta'$  and  $\eta$ - $\eta'$ - $G$  mixing scheme.

Decay	MS	$\mathcal{M}^{a+b}$	$\mathcal{M}^{c+d}$	$\mathcal{M}^{\text{anni}}$	$\mathcal{M}_{LO}$	$R_{LO}$
$K^0\eta$	1	$-1.30 + i0.04$	$0.06 - i0.11$	$-0.06 + i0.53$	$-1.30 + i0.47$	$1.69 : 0.01 : 0.29 : 1.91$
	2	$-0.80 + i0.03$	$0.03 - i0.07$	$0.01 + i0.54$	$-0.76 + i0.51$	$0.63 : 0.01 : 0.30 : 0.83$
$K^0\eta'$	1	$3.42 + i0.03$	$0.25 - i0.47$	$-0.07 - i2.85$	$3.40 - i3.29$	$11.7 : 0.29 : 8.1 : 22.4$
	2	$4.12 + i0.03$	$0.24 - i0.45$	$-0.03 - i2.94$	$4.32 - i3.37$	$17.0 : 0.27 : 8.6 : 30.0$
$K^+\eta$	1	$-1.76 - i0.37$	$0.07 - i0.14$	$0.03 + i0.57$	$-1.67 + i0.06$	$3.23 : 0.02 : 0.33 : 2.79$
	2	$-1.18 - i0.52$	$0.03 - i0.09$	$0.10 + i0.58$	$-1.05 - i0.03$	$1.66 : 0.01 : 0.35 : 1.10$
$K^+\eta'$	1	$3.65 - i0.30$	$0.26 - i0.54$	$-0.41 - i2.99$	$3.50 - i3.83$	$13.4 : 0.36 : 9.1 : 26.9$
	2	$4.44 - i0.49$	$0.25 - i0.52$	$-0.38 - i3.07$	$4.31 - i4.08$	$20.0 : 0.33 : 9.6 : 32.2$

From the numerical results as shown in Table VII, we find the following points:

- (i) For all the four considered decays, the factorizable emission diagrams in Figs. 1(a) and 1(b) provide the dominant contribution to the branching ratios. In both the MS-1 and MS-2 mixing schemes, we have

$$\frac{|\mathcal{M}^{c+d}|^2}{|\mathcal{M}^{a+b}|^2} < 0.01, \quad \frac{|\mathcal{M}^{\text{anni}}|^2}{|\mathcal{M}^{a+b}|^2} < 0.5, \quad (88)$$



for the two  $B \rightarrow K\eta$  decays, and

$$\frac{|\mathcal{M}^{c+d}|^2}{|\mathcal{M}^{a+b}|^2} < 0.03, \quad \frac{|\mathcal{M}^{\text{anni}}|^2}{|\mathcal{M}^{a+b}|^2} < 0.7, \quad (89)$$

for the two  $B \rightarrow K\eta'$  decays.

- (ii) For all four of the considered decays, one can see from Eqs.(88) and (89) that the contribution from the spectator diagrams Figs. 1(c) and 1(d) is very small in size,

$$\frac{|\mathcal{M}^{c+d}|^2}{|\mathcal{M}^{\text{LO}}|^2} < 0.03, \quad (90)$$

and therefore can be neglected safely, which is consistent with the general expectation. Since the LO part  $\mathcal{M}^{c+d}$  is already negligibly small, it is reasonable for us to neglect the corresponding higher order NLO contribution  $\mathcal{M}_{\text{NLO}}^{c+d}$  from the corresponding spectator diagrams Figs.5(a)-5(d).

- (iii) For all the four considered decays, the real parts of  $\mathcal{M}^{\text{anni}}$  are very small, but their imaginary parts are relatively large. This leads to a large strong phase, which is consistent with the general expectation.
- (iv) For the two  $B \rightarrow K\eta'$  decays, the large imaginary parts of  $\mathcal{M}^{\text{anni}}$  can also provide an effective enhancement to their branching ratios. From this point we understand that although the factorizable emission diagrams Figs. 1(a) and 1(b) provide the dominant contribution to the considered decays, but the LO contribution from the annihilation diagrams also provide an essential contribution. Therefore, the NLO contribution  $\mathcal{M}_{\text{NLO}}^{\text{anni}}$  from the corresponding annihilation diagrams as shown in Figs. 5(e)-5(h) may be comparable with other NLO parts, and thus the analytical calculations for these diagrams should be done as soon as possible.

Now we study the relative strength for all known NLO contributions from different sources and collect all numerical results in Tables VIII and IX.

In Table VIII we list the numerical values for individual decay amplitudes. The decay amplitude  $\mathcal{M}_{\text{NLOWC}}$  are obtained by evaluating the Figs. 1(a)-1(h) using the NLO Wilson coefficients  $C_i(\mu)$ , the NLO RG evolution matrix  $U(t, m, \alpha)$  and  $\alpha_s(\mu)$  at the two-loop level. The label  $\mathcal{M}_{\text{VC}}$  denotes the changes of  $\mathcal{M}_{\text{NLOWC}}$  when only the NLO vertex corrections are also included. The label  $\mathcal{M}_{\text{ql}}$  ( $\mathcal{M}_{\text{mp}}$ ) shows the changes of  $\mathcal{M}_{\text{NLOWC}}$  when only the NLO contributions from the quark-loops ( the chromo-magnetic penguin) are included. The label  $\mathcal{M}_{\text{FF}}$  shows the variation of  $\mathcal{M}_{\text{NLOWC}}$  when only the  $B \rightarrow K$  and  $B \rightarrow \eta^{(\prime)}$  transition form factors at NLO level are taken into account.

The label  $\mathcal{M}_{\text{VC+ql+mp}}$  and  $\mathcal{M}_{\text{NLO}}$  in Table VIII and  $\mathcal{M}_{\text{NLO1}}$  in Table IX are defined by the following summations:

$$\mathcal{M}_{\text{VC+ql+mp}} = \mathcal{M}_{\text{VC}} + \mathcal{M}_{\text{ql}} + \mathcal{M}_{\text{mp}}, \quad (91)$$

$$\mathcal{M}_{\text{NLO1}} = \mathcal{M}_{\text{NLOWC}} + \mathcal{M}_{\text{VC+ql+mp}}, \quad (92)$$

$$\mathcal{M}_{\text{NLO}}^{\text{tot}} = \mathcal{M}_{\text{NLO1}} + \mathcal{M}_{\text{FF}}. \quad (93)$$

Here  $\mathcal{M}_{\text{NLO1}}$  is equivalent to the total decay amplitude  $\mathcal{M}$  as defined in Eq.(76) of Ref. [12], and  $\mathcal{M}_{\text{NLO}}$  is the decay amplitude when all currently known NLO contributions are taken into account.

The ratio  $R_{\text{NLO}}$  in Table IX is defined as

$$R_{\text{NLO}} = |\mathcal{M}_{\text{LO}}|^2 : |\mathcal{M}_{\text{NLO1}}|^2 : |\mathcal{M}_{\text{NLO}}^{\text{tot}}|^2. \quad (94)$$

TABLE VIII. The numerical values (in unit of  $10^{-4}$ ) of the individual NLO contributions to the decay amplitudes, coming from different sources in the  $\eta$ - $\eta'$  and  $\eta$ - $\eta'$ - $G$  mixing scheme.

Decays	MS	$\mathcal{M}_{\text{NLOWC}}$	$\mathcal{M}_{\text{VC}}$	$\mathcal{M}_{\text{ql}}$	$\mathcal{M}_{\text{mp}}$	$\mathcal{M}_{\text{VC+ql+mp}}$	$\mathcal{M}_{\text{FF}}$
$K^0\eta$	1	$-1.54 + i0.48$	$-0.03 - i0.26$	$-0.32 - i0.44$	$0.35 - i0.27$	$-0.004 - i0.97$	$0.05 - i0.04$
	2	$-0.96 + i0.54$	$-0.07 - i0.08$	$-0.25 - i0.36$	$0.22 - i0.25$	$-0.10 - i0.68$	$-0.001 - i0.02$
$K^0\eta'$	1	$4.83 - i3.94$	$0.63 - i1.34$	$1.29 + i1.59$	$-1.35 + i0.37$	$0.57 + i0.62$	$0.50 - i0.25$
	2	$5.62 - i4.03$	$0.61 - i1.22$	$1.40 + i1.73$	$-1.47 + i0.36$	$0.54 + i0.87$	$0.47 - i0.24$
$K^+\eta$	1	$-1.65 + i0.11$	$-0.05 - i0.35$	$-0.32 - i0.44$	$0.37 - i0.27$	$0.00 - i1.06$	$0.001 - i0.18$
	2	$-1.13 + i0.06$	$-0.10 - i0.18$	$-0.25 - i0.36$	$0.26 - i0.26$	$-0.09 - i0.80$	$-0.04 - i0.13$
$K^+\eta'$	1	$4.66 - i4.34$	$0.65 - i1.38$	$1.30 + i1.59$	$-1.38 + i0.36$	$0.57 + i0.57$	$0.46 - i0.36$
	2	$5.39 - i4.57$	$0.62 - i1.29$	$1.41 + i1.73$	$-1.50 + i0.35$	$0.53 + i0.79$	$0.43 - i0.35$

TABLE IX. The numerical values of  $\mathcal{M}_{\text{LO}}$ ,  $\mathcal{M}_{\text{NLO1}}$ ,  $\mathcal{M}_{\text{NLO}}$  (in units of  $10^{-4}$ ) and the ratio  $R_{\text{NLO}}$  for  $B \rightarrow K\eta^{(\prime)}$  decays in the  $\eta$ - $\eta'$  and  $\eta$ - $\eta'$ - $G$  mixing schemes.

Decay	MS	$\mathcal{M}_{\text{LO}}$	$\mathcal{M}_{\text{NLO1}}$	$\mathcal{M}_{\text{NLO}}^{\text{tot}}$	$R_{\text{NLO}}$
$K^0\eta$	1	$-1.30 + i0.47$	$-1.54 - i0.49$	$-1.49 - i0.53$	$1.91 : 2.61 : 2.50$
	2	$-0.76 + i0.51$	$-1.05 - i0.14$	$-1.05 - i0.15$	$0.84 : 1.12 : 1.13$
$K^0\eta'$	1	$3.40 - i3.29$	$5.41 - i3.32$	$5.91 - i3.57$	$22.4 : 40.3 : 47.7$
	2	$4.32 - i3.37$	$6.16 - i3.16$	$6.63 - i3.40$	$30.0 : 47.9 : 55.5$
$K^+\eta$	1	$-1.67 - i0.06$	$-1.65 - i0.96$	$-1.65 - i1.13$	$2.79 : 3.64 : 4.00$
	2	$-1.05 - i0.03$	$-1.22 - i0.74$	$-1.26 - i0.87$	$1.10 : 2.04 : 2.35$
$K^+\eta'$	1	$3.50 - i3.83$	$5.22 - i3.77$	$5.69 - i4.13$	$26.9 : 41.5 : 49.4$
	2	$4.31 - i4.08$	$5.91 - i3.78$	$6.34 - i4.13$	$32.2 : 49.2 : 57.3$

From the numerical results as shown in Tables VII-IX, we find the following points:

- (i) For all four  $B \rightarrow K\eta^{(\prime)}$  decays, there are strong cancelations between  $\mathcal{M}_{\text{VC}}$ ,  $\mathcal{M}_{\text{ql}}$ , and  $\mathcal{M}_{\text{mp}}$ .
- (ii) For two  $B \rightarrow K\eta$  decays, the corresponding  $\mathcal{M}_{\text{FF}}$  are also much smaller in magnitude than the other NLO parts  $\mathcal{M}_{\text{VC}}$ ,  $\mathcal{M}_{\text{ql}}$  and  $\mathcal{M}_{\text{mp}}$ , and also smaller in size than their summation  $\mathcal{M}_{\text{VC+ql+mp}}$ .

- (iii) For the two  $B \rightarrow K\eta'$  decays, the corresponding  $\mathcal{M}_{\text{FF}}$  are also much smaller than the other NLO parts  $\mathcal{M}_{\text{VC}}$ ,  $\mathcal{M}_{\text{ql}}$  and  $\mathcal{M}_{\text{mp}}$ , but comparable in size with their summation  $\mathcal{M}_{\text{VC+ql+mp}}$ , and therefore all NLO contributions together provide the required enhancements to  $Br(B \rightarrow K\eta')$  to account for the measured values.
- (iv) The only missing NLO parts in the pQCD approach are  $\mathcal{M}_{\text{NLO}}^{c+d}$  from Figs. 5(a)-5(d) and  $\mathcal{M}_{\text{NLO}}^{\text{anni}}$  from Figs. 5(e)-5(h). They are most probably small in size according to the studies in this paper and the general expectations based on the isospin cancelation and power suppression.

## VI. SUMMARY

In this paper, we made a systematic study of the four  $B \rightarrow K\eta^{(\prime)}$  decays in the pQCD factorization approach. We calculated the CP-averaged branching ratios and CP-violating asymmetries of the four  $B \rightarrow K\eta^{(\prime)}$  decays in three different mixing schemes: the ordinary FKS  $\eta$ - $\eta'$  mixing scheme, the  $\eta$ - $\eta'$ - $G$  mixing scheme, and the  $\eta$ - $\eta'$ - $G$ - $\eta_c$  mixing scheme. We considered the full LO contributions and all currently known NLO contributions to  $B \rightarrow K\eta^{(\prime)}$  decays in the pQCD approach. Besides those NLO contributions considered in Ref. [12], we here took the newly known NLO part of the  $B \rightarrow (K, \eta^{(\prime)})$  transition form factors into account as well.

From our numerical calculations and phenomenological analysis, we find the following points

- (i) In all three mixing schemes considered, the NLO pQCD predictions for the branching ratios and CP-violating asymmetries agree with the data within one standard deviation, of course, this is partially due to the still large theoretical errors. However, the NLO pQCD predictions in the  $\eta$ - $\eta'$ - $G$  mixing scheme provide a nearly perfect interpretation of the measured values. The NLO pQCD predictions in MS-2 are the following:

$$\begin{aligned}
Br(B^0 \rightarrow K^0\eta) &= (1.13_{-1.01}^{+1.95}) \times 10^{-6}, \\
Br(B^0 \rightarrow K^0\eta') &= (66.5_{-19.4}^{+25.9}) \times 10^{-6}, \\
Br(B^\pm \rightarrow K^\pm\eta) &= (2.36_{-1.50}^{+2.63}) \times 10^{-6}, \\
Br(B^\pm \rightarrow K^\pm\eta') &= (67.3_{-19.4}^{+26.0}) \times 10^{-6},
\end{aligned} \tag{95}$$

for branching ratios, and

$$\begin{aligned}
\mathcal{A}_{CP}^{\text{dir}}(B^\pm \rightarrow K^\pm\eta) &= (-22.9_{-19.1}^{+15.2}) \times 10^{-2}, \\
\mathcal{A}_{CP}^{\text{dir}}(B^\pm \rightarrow K^\pm\eta') &= (-5.5_{-1.9}^{+1.9}) \times 10^{-2}, \\
\mathcal{A}_{CP}^{\text{dir}}(B^0 \rightarrow K_S^0\eta) &= (-16.0_{-14.3}^{+7.9}) \times 10^{-2}, \\
\mathcal{A}_{CP}^{\text{mix}}(B^0 \rightarrow K_S^0\eta) &= (66.7_{-8.5}^{+3.7}) \times 10^{-2}, \\
\mathcal{A}_{CP}^{\text{dir}}(B^0 \rightarrow K_S^0\eta') &= (3.3 \pm 0.3) \times 10^{-2}, \\
\mathcal{A}_{CP}^{\text{mix}}(B^0 \rightarrow K_S^0\eta') &= (70.0 \pm 0.3) \times 10^{-2},
\end{aligned} \tag{96}$$

for the CP-violating asymmetries, where the individual theoretical errors have been combined in quadrature.

- (ii) For the  $B^0 \rightarrow K^0 \eta'$  and  $B^+ \rightarrow K^+ \eta'$  decays, the NLO contributions provide significant enhancements to their branching ratios. In the  $\eta$ - $\eta'$ - $G$  mixing scheme, for example, the NLO contribution provides a 89% (73%) enhancement to  $Br(B^0 \rightarrow K^0 \eta')$  ( $Br(B^+ \rightarrow K^+ \eta')$ ) with respect to the LO prediction, such enhancements play a key role in our effort to resolve the  $K \eta^{(\prime)}$  puzzle and to understand the pattern of the  $Br(B \rightarrow K \eta^{(\prime)})$ .
- (iii) For the  $B^0 \rightarrow K^0 \eta$  and  $B^+ \rightarrow K^+ \eta$  decays, the inclusion of the NLO contributions only leads to a relatively small change to their branching ratios, but the resulting variations are in the right direction and helpful for us in improving the consistency between the pQCD predictions and the measured values. In the  $\eta$ - $\eta'$ - $G$  mixing scheme, for instance, the central values of the pQCD predictions are  $Br(B^0 \rightarrow K^0 \eta) = 0.90 \times 10^{-6}$  and  $Br(B^+ \rightarrow K^+ \eta) = 1.98 \times 10^{-6}$  at the leading order, these changed to  $Br(B^0 \rightarrow K^0 \eta) = 1.13 \times 10^{-6}$  and  $Br(B^+ \rightarrow K^+ \eta) = 2.36 \times 10^{-6}$  when the NLO contributions were taken into account, while the corresponding measured values are  $1.23^{+0.27}_{-0.23} \times 10^{-6}$  and  $2.36^{+0.22}_{-0.21} \times 10^{-6}$  respectively.
- (iv) By comparing the pQCD predictions as given in the “NLO1” and “NLO” columns in Tables II-IV, one can directly see the effects of NLO form factors: the NLO part  $\mathcal{M}_{\text{FF}}$  of the  $B \rightarrow K$  and  $B \rightarrow \eta^{(\prime)}$  form factors can produce an about 20% enhancement to the branching ratios  $Br(B \rightarrow K \eta^{(\prime)})$ , which plays an important role in closing the gap between the pQCD predictions and the relevant data.
- (v) In the  $\eta$ - $\eta'$ - $G$ - $\eta_c$  mixing scheme, the decay chain  $B \rightarrow K \eta_c \rightarrow K \eta^{(\prime)}$  can provide an effective enhancement to the branching ratios at the leading-order, but when the large NLO contributions are taken into account, the effects of the  $\eta_c$  component become unimportant.
- (vi) For  $B^\pm \rightarrow K^\pm \eta$  decays, the LO pQCD predictions for  $\mathcal{A}_{CP}^{\text{dir}}$  in all three mixing schemes have a sign opposite that of the measured value. The inclusion of the NLO contributions changed the sign of the pQCD predictions for  $\mathcal{A}_{CP}^{\text{dir}}$ , while the NLO pQCD predictions for  $\mathcal{A}_{CP}^{\text{dir}}(B^\pm \rightarrow K^\pm \eta)$  in the cases of the MS-1 and MS-2 are now becoming consistent with the data within one standard deviation, but the NLO pQCD prediction for  $\mathcal{A}_{CP}^{\text{dir}}(B^\pm \rightarrow K^\pm \eta)$  in the MS-3 case is still much smaller in magnitude than the measured value.
- (vii) For  $\mathcal{A}_{CP}^{\text{dir}}(B^\pm \rightarrow K^\pm \eta')$ , the NLO pQCD predictions agree with the data within one standard deviation, while the consistency between the pQCD predictions and the data is improved by the inclusion of the NLO contributions.
- (viii) For the direct and mixing-induced CP-violating asymmetries  $\mathcal{A}_{CP}^{\text{dir}}(B^0 \rightarrow K_S^0 \eta^{(\prime)})$  and  $\mathcal{A}_{CP}^{\text{mix}}(B^0 \rightarrow K_S^0 \eta^{(\prime)})$ , the pQCD predictions have a weak dependence on the NLO contributions and the choice of different mixing schemes. For  $\mathcal{A}_{CP}^{\text{dir,mix}}(B^0 \rightarrow K_S^0 \eta')$ , for example, the NLO pQCD predictions are  $\mathcal{A}_{CP}^{\text{dir}}(B^0 \rightarrow K_S^0 \eta') \approx 3\%$  and  $\mathcal{A}_{CP}^{\text{mix}}(B^0 \rightarrow K_S^0 \eta') \approx 70\%$ , which are well consistent with the measured values of  $(1 \pm 9)\%$  and  $(64 \pm 11)\%$  respectively.
- (ix) The factorizable emission diagrams Figs. 1(a) and 1(b) provide the dominant contribution to the considered decays. The LO contribution  $\mathcal{M}^{c+d}$  from the spectator dia-

grams Figs. 1(c) and 1(d) is already less than 3% of the total contribution, the next-to-leading order contributions  $\mathcal{M}_{NLO}^{c+d}$  from the Figs. 5(a)-5(d) are the higher-order contributions and therefore should be smaller than their LO counterpart  $\mathcal{M}^{c+d}$ . Consequently, it is reasonable for us to neglect  $\mathcal{M}_{NLO}^{c+d}$  from the spectator diagrams Figs. 5(a)-5(d).

- (x) The real part of  $\mathcal{M}^{\text{anni}}$  is always negligibly small, but its imaginary part is relatively large and leads to a large strong phase, which can also produce an effective enhancement to the branching ratios of the considered decays. Although  $|\mathcal{M}_{NLO}^{\text{anni}}|$  is most possibly much smaller than its LO counterpart  $|\mathcal{M}^{\text{anni}}|$ , but the still missing NLO contribution  $\mathcal{M}_{NLO}^{\text{anni}}$  from Figs. 5(e)-5(h) may be comparable in size with  $\mathcal{M}_{\text{FF}}$ , and should be calculated as soon as possible.

## ACKNOWLEDGMENTS

The authors are very grateful to Hsiang-nan Li, Cai-Dian Lu and Xin Liu for helpful discussions. This work is supported by the National Natural Science Foundation of China under the Grant Nos. 10975074 and 11235005; and by the Project on Graduate Students Education and Innovation of Jiangsu Province, under Grant No. CXLX11-0867.

## Appendix A: Distribution Amplitudes

The expressions for the relevant distribution amplitudes (DAs) of the K meson are the following [34, 39]:

$$\phi_K^A(x) = \frac{f_K}{2\sqrt{2N_c}} 6x(1-x) \left[ 1 + a_1^K C_1^{3/2}(t) + a_2^K C_2^{3/2}(t) + a_4^K C_4^{3/2}(t) \right], \quad (\text{A1})$$

$$\phi_K^P(x) = \frac{f_K}{2\sqrt{2N_c}} \left\{ 1 + (30\eta_3 - \frac{5}{2}\rho_K^2) C_2^{1/2}(t) - 3 \left[ \eta_3\omega_3 + \frac{9}{20}\rho_K^2(1 + 6a_2^K) \right] C_4^{1/2}(t) \right\} \quad (\text{A2})$$

$$\phi_K^T(x) = -\frac{f_K}{2\sqrt{2N_c}} t \left[ 1 + 6(5\eta_3 - \frac{1}{2}\eta_3\omega_3 - \frac{7}{20}\rho_K^2 - \frac{3}{5}\rho_K^2 a_2^K)(1 - 10x + 10x^2) \right], \quad (\text{A3})$$

with the mass ratio  $\rho_K = m_K/m_{0K}$ . The Gegenbauer moments are of the form [34]:

$$a_1^K = 0.2, \quad a_2^K = 0.25, \quad a_4^K = -0.015. \quad (\text{A4})$$

The values of the other parameters are  $\eta_3 = 0.015$  and  $\omega = -3.0$ . Finally, the Gegenbauer polynomials  $C_n^\nu(t)$  are given as:

$$\begin{aligned} C_2^{1/2}(t) &= \frac{1}{2}(3t^2 - 1), & C_4^{1/2}(t) &= \frac{1}{8}(3 - 30t^2 + 35t^4), \\ C_1^{3/2}(t) &= 3t, & C_2^{3/2}(t) &= \frac{3}{2}(5t^2 - 1), \\ C_4^{3/2}(t) &= \frac{15}{8}(1 - 14t^2 + 21t^4), \end{aligned} \quad (\text{A5})$$

with  $t = 2x - 1$ .

The distribution amplitudes  $\phi_{\eta_q}^{A,P,T}$  are given as [34]:

$$\phi_{\eta_q}^A(x) = \frac{f_q}{2\sqrt{2N_c}} 6x(1-x) \left[ 1 + a_1^{\eta_q} C_1^{3/2}(2x-1) + a_2^{\eta_q} C_2^{3/2}(2x-1) + a_4^{\eta_q} C_4^{3/2}(2x-1) \right], \quad (\text{A6})$$

$$\phi_{\eta_q}^P(x) = \frac{f_q}{2\sqrt{2N_c}} \left[ 1 + (30\eta_3 - \frac{5}{2}\rho_{\eta_q}^2) C_2^{1/2}(2x-1) - 3 \left\{ \eta_3\omega_3 + \frac{9}{20}\rho_{\eta_q}^2(1+6a_2^{\eta_q}) \right\} C_4^{1/2}(2x-1) \right], \quad (\text{A7})$$

$$\phi_{\eta_q}^T(x) = \frac{f_q}{2\sqrt{2N_c}} (1-2x) \left[ 1 + 6 \left( 5\eta_3 - \frac{1}{2}\eta_3\omega_3 - \frac{7}{20}\rho_{\eta_q}^2 - \frac{3}{5}\rho_{\eta_q}^2 a_2^{\eta_q} \right) \cdot (1-10x+10x^2) \right], \quad (\text{A8})$$

where  $\rho_{\eta_q} = 2m_q/m_{q\bar{q}}$ ,  $a_1^{\eta_q} = a_1^\pi = 0$ ,  $a_2^{\eta_q} = a_2^\pi = 0.44 \pm 0.22$ ,  $a_4^{\eta_q} = a_4^\pi = 0.25$ , and the Gegenbauer polynomials  $C_n^\nu(t)$  have been given in Eq. (A5). As for the wave function and the corresponding DAs of the  $s\bar{s}$  components, we also use the same form as  $q\bar{q}$  but with some parameters changed:  $\rho_{\eta_s} = 2m_s/m_{s\bar{s}}$ ,  $a_i^{\eta_s} = a_i^{\eta_q}$  for  $i = 1, 2, 4$ .

## Appendix B: Related Hard Functions

The hard scales appearing in the decay amplitudes are chosen as

$$\begin{aligned} t_a &= \max\{\sqrt{x_3}M_B, 1/b_1, 1/b_3\}, \\ t'_a &= \max\{\sqrt{x_1}M_B, 1/b_1, 1/b_3\}, \\ t_b &= \max\{\sqrt{x_1x_3}M_B, \sqrt{|1-x_1-x_2|x_3}M_B, 1/b_1, 1/b_2\}, \\ t'_b &= \max\{\sqrt{x_1x_3}M_B, \sqrt{|x_1-x_2|x_3}M_B, 1/b_1, 1/b_2\}, \\ t_c &= \max\{\sqrt{1-x_3}M_B, 1/b_2, 1/b_3\}, \\ t'_c &= \max\{\sqrt{x_2}M_B, 1/b_2, 1/b_3\}, \\ t_d &= \max\{\sqrt{x_2(1-x_3)}M_B, \sqrt{1-(1-x_1-x_2)x_3}M_B, 1/b_1, 1/b_2\}, \\ t'_d &= \max\{\sqrt{x_2(1-x_3)}M_B, \sqrt{|x_1-x_2|(1-x_3)}M_B, 1/b_1, 1/b_2\}, \\ t_e &= \max\{\sqrt{x_3(1-r_{\eta_c}^2)}M_B, 1/b_1, 1/b_3\}, \\ t'_e &= \max\{\sqrt{x_1(1-r_{\eta_c}^2)}M_B, 1/b_1, 1/b_3\}, \\ t_f &= \max\{\sqrt{x_1x_3(1-r_{\eta_c}^2)}M_B, \sqrt{|(-1+x_1+x_2)[x_3+(1-x_2-x_3)r_{\eta_c}^2]+r_{\eta_c}^2}|M_B, \\ &\quad 1/b_1, 1/b_2\}, \\ t'_f &= \max\{\sqrt{x_1x_3(1-r_{\eta_c}^2)}M_B, \sqrt{|(x_1-x_2)[x_3+(x_2-x_3)r_{\eta_c}^2]+r_{\eta_c}^2}|M_B, \\ &\quad 1/b_1, 1/b_2\}. \end{aligned} \quad (\text{B1})$$

The hard functions  $h_i$ s appearing in the decay amplitudes are defined by

$$\begin{aligned}
h_e(x_1, x_3, b_1, b_3) &= [\theta(b_1 - b_3)I_0(\sqrt{x_3}M_B b_3)K_0(\sqrt{x_3}M_B b_1) \\
&\quad + \theta(b_3 - b_1)I_0(\sqrt{x_3}M_B b_1)K_0(\sqrt{x_3}M_B b_3)] K_0(\sqrt{x_1 x_3}M_B b_1)S_t(x_3), \\
h_n(x_1, x_2, x_3, b_1, b_2) &= [\theta(b_2 - b_1)K_0(\sqrt{x_1 x_3}M_B b_2)I_0(\sqrt{x_1 x_3}M_B b_1) \\
&\quad + \theta(b_1 - b_2)K_0(\sqrt{x_1 x_3}M_B b_1)I_0(\sqrt{x_1 x_3}M_B b_2)] \\
&\quad \times \begin{cases} \frac{i\pi}{2}H_0^{(1)}(\sqrt{(x_2 - x_1)x_3}M_B b_2), & x_1 - x_2 < 0 \\ K_0(\sqrt{(x_1 - x_2)x_3}M_B b_2), & x_1 - x_2 > 0 \end{cases}, \tag{B2}
\end{aligned}$$

$$\begin{aligned}
h_a(x_2, x_3, b_2, b_3) &= \left(\frac{i\pi}{2}\right)^2 S_t(x_3) \left[ \theta(b_2 - b_3)H_0^{(1)}(\sqrt{x_3}M_B b_2)J_0(\sqrt{x_3}M_B b_3) \right. \\
&\quad \left. + \theta(b_3 - b_2)H_0^{(1)}(\sqrt{x_3}M_B b_3)J_0(\sqrt{x_3}M_B b_2) \right] H_0^{(1)}(\sqrt{x_2 x_3}M_B b_2), \\
h_{na}(x_1, x_2, x_3, b_1, b_2) &= \frac{i\pi}{2} \left[ \theta(b_1 - b_2)H_0^{(1)}(\sqrt{x_2(1 - x_3)}M_B b_1)J_0(\sqrt{x_2(1 - x_3)}M_B b_2) \right. \\
&\quad \left. + \theta(b_2 - b_1)H_0^{(1)}(\sqrt{x_2(1 - x_3)}M_B b_2)J_0(\sqrt{x_2(1 - x_3)}M_B b_1) \right] \\
&\quad \times K_0(\sqrt{1 - (1 - x_1 - x_2)x_3}M_B b_1), \tag{B3}
\end{aligned}$$

$$\begin{aligned}
h'_{na}(x_1, x_2, x_3, b_1, b_2) &= \frac{i\pi}{2} \left[ \theta(b_1 - b_2)H_0^{(1)}(\sqrt{x_2(1 - x_3)}M_B b_1)J_0(\sqrt{x_2(1 - x_3)}M_B b_2) \right. \\
&\quad \left. + \theta(b_2 - b_1)H_0^{(1)}(\sqrt{x_2(1 - x_3)}M_B b_2)J_0(\sqrt{x_2(1 - x_3)}M_B b_1) \right] \\
&\quad \times \begin{cases} \frac{i\pi}{2}H_0^{(1)}(\sqrt{(x_2 - x_1)(1 - x_3)}M_B b_1), & x_1 - x_2 < 0 \\ K_0(\sqrt{(x_1 - x_2)(1 - x_3)}M_B b_1), & x_1 - x_2 > 0 \end{cases}, \tag{B4}
\end{aligned}$$

where  $H_0^{(1)}(z) = J_0(z) + i Y_0(z)$ .

$$\begin{aligned}
h'_e(x_1, x_3, b_1, b_3) &= [\theta(b_1 - b_3)I_0(\sqrt{\alpha}M_B b_3)K_0(\sqrt{\alpha}M_B b_1) \\
&\quad + \theta(b_3 - b_1)I_0(\sqrt{\alpha}M_B b_1)K_0(\sqrt{\alpha}M_B b_3)] K_0(\sqrt{\beta}M_B b_1)S_t(x_3), \tag{B5}
\end{aligned}$$

where  $\alpha = x_3(1 - r_{\eta_c}^2)$ ,  $\beta = x_1 x_3(1 - r_{\eta_c}^2)$ .

$$\begin{aligned}
h'_n(x_1, x_2, x_3, b_1, b_2) &= \left[ \theta(b_2 - b_1)K_0(\sqrt{\alpha'}M_B b_2)I_0(\sqrt{\alpha'}M_B b_1) \right. \\
&\quad \left. + \theta(b_1 - b_2)K_0(\sqrt{\alpha'}M_B b_1)I_0(\sqrt{\alpha'}M_B b_2) \right] \\
&\quad \times \begin{cases} \frac{i\pi}{2}H_0^{(1)}(\sqrt{|\beta'^2|}M_B b_2), & \beta'^2 < 0 \\ K_0(\sqrt{|\beta'^2|}M_B b_2), & \beta'^2 > 0 \end{cases}, \tag{B6}
\end{aligned}$$

where  $\alpha' = x_1 x_3(1 - r_{\eta_c}^2)$ , and  $\beta'^2 = (x_1 - x_2)[x_2 r_{\eta_c}^2 + x_3(1 - r_{\eta_c}^2)] + r_{\eta_c}^2$ .

The function  $S_t(x)$  has been parametrized as [32, 40]

$$S_t(x) = \frac{2^{1+2c}\Gamma(3/2 + c)}{\sqrt{\pi}\Gamma(1 + c)}[x(1 - x)]^c, \tag{B7}$$

with  $c = 0.3$ .

The evolution factors  $E_e^{(\prime)}$ , and  $E_a^{(\prime)}$ , appearing in the decay amplitudes are given by

$$\begin{aligned} E_e(t) &= \alpha_s(t) \exp[-S_B(t) - S_3(t)], \\ E_e'(t) &= \alpha_s(t) \exp[-S_B(t) - S_2(t) - S_3(t)]|_{b_1=b_3}, \\ E_a(t) &= \alpha_s(t) \exp[-S_2(t) - S_3(t)], \\ E_a'(t) &= \alpha_s(t) \exp[-S_B(t) - S_2(t) - S_3(t)]|_{b_2=b_3}, \end{aligned} \quad (\text{B8})$$

where the Sudakov exponents are defined as [5, 6, 9]

$$\begin{aligned} S_B(t) &= s\left(x_1 \frac{M_B}{\sqrt{2}}, b_1\right) + \frac{5}{3} \int_{1/b_1}^t \frac{d\bar{\mu}}{\bar{\mu}} \gamma_q(\alpha_s(\bar{\mu})), \\ S_2(t) &= s\left(x_2 \frac{M_B}{\sqrt{2}}, b_2\right) + s\left((1-x_2) \frac{M_B}{\sqrt{2}}, b_2\right) + 2 \int_{1/b_2}^t \frac{d\bar{\mu}}{\bar{\mu}} \gamma_q(\alpha_s(\bar{\mu})), \end{aligned} \quad (\text{B9})$$

with the quark anomalous dimension  $\gamma_q = -\alpha_s/\pi$ . Replacing the variables  $(x_2, b_2)$  in  $S_2$  by  $(x_3, b_3)$ , we get the expression for  $S_3$ . At the one-loop order, the explicit expression of the function  $s(Q, b)$  is [5, 6]:

$$\begin{aligned} s(Q, b) &= \frac{A^{(1)}}{2\beta_1} \hat{q} \ln\left(\frac{\hat{q}}{\hat{b}}\right) - \frac{A^{(1)}}{2\beta_1} (\hat{q} - \hat{b}) + \frac{A^{(2)}}{4\beta_1^2} \left(\frac{\hat{q}}{\hat{b}} - 1\right) \\ &\quad - \left[ \frac{A^{(2)}}{4\beta_1^2} - \frac{A^{(1)}}{4\beta_1} \ln\left(\frac{e^{2\gamma_E-1}}{2}\right) \right] \ln\left(\frac{\hat{q}}{\hat{b}}\right) + \dots \end{aligned} \quad (\text{B10})$$

where the variables are defined by

$$\hat{q} \equiv \ln[Q/(\sqrt{2}\Lambda)], \quad \hat{b} \equiv \ln[1/(b\Lambda)], \quad (\text{B11})$$

and the coefficients  $A^{(i)}$  and  $\beta_1$  are of the form

$$\beta_1 = \frac{33-2n_f}{12}, \quad A^{(1)} = \frac{4}{3}, \quad A^{(2)} = \frac{67}{9} - \frac{\pi^2}{3} - \frac{10}{27}n_f + \frac{8}{3}\beta_1 \ln\left(\frac{1}{2}e^{\gamma_E}\right), \quad (\text{B12})$$

where  $n_f$  is the number of the quark flavors and  $\gamma_E$  is the Euler constant.

- 
- [1] B.H. Behrens *et al.*, (CLEO Collaboration), Phys. Rev. Lett. **80**, 3710 (1998).
  - [2] A.L. Kagan and A.A. Petrov, arXiv: hep-ph/9707354; S. Khalil and E. Kou, Phys. Rev. Lett. **91**, 241602 (2003).
  - [3] G.R. Lu, Z.J. Xiao, H.K. Guo and L.X. Lü, J. Phys. G **25**, L85 (1999); Z.J. Xiao, K.T. Chao and C.S. Li, Phys. Rev. D **65**, 114021(2002); Z.J. Xiao and W.J. Zou, Phys. Rev. D **70**, 094008 (2004).
  - [4] M.Z. Yang and Y.D. Yang, Nucl. Phys. B **609**, 469 (2001);
  - [5] Y.-Y. Keum, H.N. Li and A.I. Sanda, Phys. Rev. D **63**, 054008 (2001).
  - [6] C.D. Lü, K. Ukai and M.Z. Yang, Phys. Rev. D **63**, 074009 (2001).
  - [7] M. Beneke and M. Neubert, Nucl. Phys. B **651**, 225 (2003).
  - [8] E. Kou and A. Sanda, Phys. Lett. B **525**, 240 (2002).



- [9] H.N. Li, Prog. Part. & Nucl. Phys. **51**, 85 (2003) and references therein.
- [10] Y. Amhis *et al.*, (Heavy Flavor Averaging Group), arXiv:1207.1158 [hep-ex] and online update at <http://www.slac.stanford.edu/xorg/hfag>.
- [11] J. Beringer *et al.* (Particle Data Group), Phys. Rev. D **86**, 010001 (2012).
- [12] Z.J. Xiao, Z.Q. Zhang, X. Liu, and L.B. Guo, Phys. Rev. D **78**, 114001 (2008).
- [13] Th. Feldmann, P. Kroll, and B. Stech, Phys. Rev. D **58**, 114006 (1998); Phys. Lett. B **449**, 339 (1999).
- [14] H.N. Li, Y.L. Shen, and Y.M. Wang, Phys. Rev. D **85**, 074004 (2012).
- [15] X. Liu, H.N. Li, and Z.J. Xiao, Phys. Rev. D **86**, 011501(R)(2012).
- [16] H.Y. Cheng, H.N. Li, and K.F. Liu, Phys. Rev. D **79**, 014024 (2009).
- [17] Y.Y. Charng, T. Kurimoto, and H.N. Li, Phys. Rev. D **74**, 074024 (2006); **78**, 059901(E) (2008).
- [18] Y.D. Tsai, H.N. Li, and Q. Zhao, Phys. Rev. D **85**, 034002 (2012).
- [19] X. Liu, H.S. Wang, Z.J. Xiao, L.B. Guo, and C.D. Lü, Phys. Rev. D **73**, 074002 (2006); H.S. Wang, X. Liu, Z.J. Xiao, L.B. Guo, and C.D. Lü, Nucl. Phys. B **738**, 243 (2006); Z.J. Xiao, D.Q. Guo, and X.F. Chen, Phys. Rev. D **75**, 014018 (2007); D.Q. Guo, X.F. Chen, and Z.J. Xiao, Phys. Rev. D **75**, 054033 (2007); X.F. Chen, D.Q. Guo, and Z.J. Xiao, Eur. Phys. J. C **50**, 363 (2007).
- [20] A. Ali, G. Kramer, Y. Li, C.D. Lü, Y.L. Shen, W. Wang, and Y.M. Wang, Phys. Rev. D **76**, 074018 (2007).
- [21] H.N. Li, S. Mishima, and A.I. Sanda, Phys. Rev. D **72**, 114005 (2005), and references therein.
- [22] H.Y. Cheng, K.C. Yang, Phys. Rev. D **63**, 074011 (2001).
- [23] X. Liu, Z.Q. Zhang, and Z.J. Xiao, Chin. Phys. C **34**, 937 (2010).
- [24] X. Liu, Z.J. Xiao, and C.D. Lu, Phys. Rev. D **81**, 014022(2010); X. Liu and Z.J. Xiao, Phys. Rev. D **81**, 074017 (2010); Phys. Rev. D **82**, 054029(2010); J. Phys. G **38**, 035009 (2011); Z.J. Xiao and X. Liu, Phys. Rev. D **84**, 074033 (2011).
- [25] Z.J. Xiao, W.F. Wang, and Y.Y. Fan, Phys. Rev. D **85**, 094003 (2012).
- [26] Y. Li, C.D. Lü, Z.J. Xiao, and X.Q. Yu, Phys. Rev. D **70**, 034009 (2004).
- [27] H.N. Li, Y.L. Shen, Y.M. Wang, and H. Zou, Phys. Rev. D **83**, 054029 (2011).
- [28] J.C. Collins and D.E. Soper, Nucl. Phys. B **193**, 381 (1981); J. Botts and G. Sterman, Nucl. Phys. B **325**, 62 (1989).
- [29] G. Buchalla, A.J. Buras, and M.E. Lautenbacher, Rev. Mod. Phys. **68**, 1125 (1996).
- [30] F. Ambrosino *et al.*, (KLOE Collaboration), Phys. Lett. B **648**, 267 (2007); R. Escribano and J. Nadal, J. High Energy Phys. **05** (2007) 006.
- [31] Y.Y. Keum, H.N. Li, and A.I. Sanda, Phys. Lett. B **504**, 6 (2001); C.H. Chen and H.N. Li, Phys. Rev. D **63**, 014003 (2000); C.D. Lü and M.Z. Yang, Eur. Phys. J. C **28**, 515 (2003).
- [32] T. Kurimoto, H.N. Li, and A.I. Sanda, Phys. Rev. D **65**, 014007 (2001).
- [33] K.C. Bowler *et al.*, Phys. Lett. B **486**, 111 (2000).
- [34] P. Ball, V.M. Braun, Y. Koike, and K. Tanaka, Nucl. Phys. B **529**, 323 (1998); P. Ball, J. High Energy Phys. 09 (1998) 005; J. High Energy Phys. 01 (1999) 010.
- [35] A.E. Bondar, V.L. Chernyak, Phys. Lett. B **612**, 215 (2005).
- [36] M. Beneke, G. Buchalla, M. Neubert, and C.T. Sachrajda, Phys. Rev. Lett. **83**, 1914 (1999); Nucl. Phys. B **591**, 313 (2000).
- [37] M. Beneke and M. Neubert, Nucl. Phys. B **675**, 333 (2003).

- [38] S. Mishima and A.I. Sanda, Prog. Theor. Phys. **110**, 549 (2003).
- [39] P. Ball and R. Zwicky, Phys. Rev. D **71**, 014015 (2005); J. High Energy Phys. 0604 (2006) 046.
- [40] H.N. Li, Phys. Rev. D **66**, 094010 (2002).